Technische Universität München

Single-Cell RNA Sequencing Analysis Revealed Cellular Heterogeneity of Human Abdominal Aortic Aneurysm

Zhiyuan WU

Fakultät für Medizin

Technische Universität München

2021.08

Technische Universität München

Klinik und Poliklinik für Vaskuläre und Endovaskuläre Chirurgie
Klinikum rechts der Isar der Technischen Universität München
(Vorstand: Prof. Dr. Hans–Henning Eckstein)

Single-Cell RNA Sequencing Analysis Revealed Cellular Heterogeneity of Human Abdominal Aortic Aneurysm

Zhiyuan WU

Vollständiger Abdruck der von der Fakultät für Medizin der Technischen Universität München zur Erlangung des akademischen Grades eines Doktors der Medizin genehmigten Dissertation.

Vorsitzender: Prof. Dr. Florian Eyer
Prüfer der Dissertation:

1. **Prof. Dr. Lars Maegdefessel**
2. **Prof. Dr. Hendrik Sager**

Die Dissertation wurde am 09.12.2020 bei der Technischen Universität München eingereicht und durch die Fakultät für Medizin am 13.07.2021 angenommen.

TABLE OF CONTENTS

ABSTRACT

Background:
Abdominal aortic aneurysm (AAA) poses a great threat to patients. AAA is mostly asymptomatic and often incidentally found on ultrasound, computerized tomography (CT) or X-rays scans. Currently there are no pharmacological treatments ameliorating disease prognosis. Single-cell RNA sequencing (scRNA-seq) stands now at the forefront of phenotyping experiments and has been widely used in the quest for targets improving molecular diagnostics, as well as paving the way for novel therapeutic strategies. The aim of my thesis project was to reveal the cellular heterogeneity of AAA at the single-cell level.

Materials and Methods:
Human AAA samples were collected from patients undergoing open repair surgery. In particular, for each patient, the aneurysm non-dilated neck was dissected from the enlarged aortic portion. Non-dilated and dilated abdominal aorta fragments were subsequently digested and scRNA-seq libraries were prepared according to 10X Genomics Chromium Platform manufacturer's instructions. RNA sequencing was performed with the NovaSeq6000 platform and downstream *in silico* analysis were carried out by using R.

Results:
After quality check and filtering, more than 900 cells were included for analysis. Unbiased clustering analysis identified 15 distinct cell clusters, mainly including macrophages, monocytes, dendritic cells, vascular muscle smooth cells (VSMC), endothelial cells (EC), fibroblasts, T cells, B cells and plasma cells. Further analysis revealed 4 distinct subclusters in macrophages, 3 different VSMC subpopulations, and 3 fibroblast subsets. The 4 macrophage clusters decreased from the non-dilated part to the dilated part, though, they still accounted for most of the immune cells in AAA. A "modulated VSMC" was also detected in this dataset and featured at its transcriptional profiles, which may play important role in AAA progression.

Conclusion:
Current single-cell data analysis revealed the heterogeneity in AAA and characterized the subpopulations of macrophages and VSMCs, along with their possible functions during the AAA development and progression.

Keywords:
Single-cell RNA Sequencing; Abdominal Aortic Aneurysm; Macrophages; Vascular Smooth Muscle Cell; Cellular Heterogeneity.

LIST OF ABBREVIATIONS

AAA	Abdominal Aortic Aneurysm
ACKR3	Atypical Chemokine Receptor 3
ACTA2	Actin Alpha 2, Smooth Muscle
ADAMTS1	ADAM Metallopeptidase with Thrombospondin Type 1 Motif 1
AFs	Adventitial Fibroblasts
AKAP12	A-Kinase Anchoring Protein 12
AREG	Amphiregulin
BC	B Cells
C11orf96	Chromosome 11 Open Reading Frame 96
C1QA	Complement C1q A Chain
C1QB	Complement C1q B Chain
C1QC	Complement C1q C Chain
CCL20	C-C Motif Chemokine Ligand 20
CCL4	C-C Motif Chemokine Ligand 4
CCR7	C-C Motif Chemokine Receptor 7
CD14	Cluster of Differentiation 14
CD36	Cluster of Differentiation 36
CD4	Cluster of Differentiation 4
CD68	Cluster of Differentiation 68
CD74	Cluster of Differentiation 74
CD79A	Cluster of Differentiation 79A
CD8	Cluster of Differentiation 8
CDH5	Cadherin 5
CLEC10A	C-Type Lectin Domain Containing 10A
COL14A1	Collagen Type XIV Alpha 1 Chain
COL18A1	Collagen Type XVIII Alpha 1
COL1A1	Collagen Type I Alpha 1 Chain
COL3A1	Collagen Type III Alpha 1 Chain
COL4A1	Collagen Type IV Alpha 1 Chain
COL4A2	Collagen Type IV Alpha 2 Chain
COL6A1	Collagen Type VI Alpha 1 Chain
COL6A2	Collagen Type VI Alpha 2 Chain
CRLF1	Cytokine Receptor Like Factor 1
CTSB	Cathepsin B
CTSD	Cathepsin D
CTSZ	Cathepsin Z
CXCL2	C-X-C Motif Chemokine Ligand 2
CXCL3	C-X-C Motif Chemokine Ligand 3
CXCL5	C-X-C Motif Chemokine Ligand 5
CXCL8	C-X-C Motif Chemokine Ligand 8

CXCL14	C-X-C Motif Chemokine Ligand 14
DC	Dendritic Cell
DCN	Decorin
DEGs	Differently Expressed Genes
DM	Dilated Part of AAA with Enzymes of Milt kit
DMEM	Dulbecco's Modified Eagle's Medium
DP	Dilated Part of AAA
DS	Dilated Part of AAA with Self-prepared Enzymes
EC	Endothelial Cells
ECM	Extracellular Matrix
ECSCR	Endothelial Cell Surface Expressed Chemotaxis and Apoptosis Regulator
ENG	Endoglin
EREG	Epiregulin
ETS2	ETS Proto-Oncogene 2, Transcription Factor
EVAR	Endovascular Aortic Repair
F13A1	Coagulation Factor XIII A Chain
FABP4	Fatty Acid Binding Protein 4
FACS	Fluorescence Assisted Cell Sorting
FBLN1	Fibulin 1
FBS	Fetal Bovine Serum
FC	Fold Change
FCGR3A	Fc Fragment of IgG Receptor IIIa
FFPE	Formalin-Fixed Paraffin-Embedded
FKBP4	FKBP Prolyl Isomerase 4
FN1	Fibronectin 1
FOLR2	Folate Receptor Beta
GEM	Gel Bead-in-Emulsions
GIMAP4	GTPase, IMAP Family Member 4
GIMAP7	GTPase, IMAP Family Member 7
GLT8D1	Glycosyltransferase 8 Domain Containing
GO	Gene Ontology
GPC3	Glypican 3
GZMA	Granzyme A
H19	H19 mprinted maternally expressed transcript
HBEGF	Heparin Binding EGF Like Growth Factor
HLA-DPA1	Major Histocompatibility Complex, Class II, DP Alpha 1
HLA-DPB1	Major Histocompatibility Complex, Class II, DP Beta 1
HLA-DQA1	Major Histocompatibility Complex, Class II, DQ Alpha 1
HLA-DQB1	Major Histocompatibility Complex, Class II, DQ Beta 1
HLA-DRA	Major Histocompatibility Complex, Class II, DR Alpha
HLA-DRB1	Major Histocompatibility Complex, Class II, DR Beta 1
HMOX1	Heme Oxygenase 1

IER3	Immediate Early Response 3
IGFBP3	Insulin Like Growth Factor Binding Protein 3
IL1B	Interleukin 1 Beta
LCIA	Left Common Iliac Artery
LGALS3	Galectin 3
LRA	Left Renal Artery
LRRC28	Leucine Rich Repeat Containing 28
LUM	Lumican
NDP	Nondilated Part of AAA
MALAT1	Metastasis Associated Lung Adenocarcinoma Transcript 1
MHC	Major Histocompatibility Complex
MMP12	Matrix Metallopeptidase 12
MMP14	Matrix Metallopeptidase 14
MMP19	Matrix Metallopeptidase 19
MMP3	Matrix Metallopeptidase 3
MMP9	Matrix Metallopeptidase 9
MMRN2	Multimerin 2
Mono	Monocyte
MS4A1	Membrane Spanning 4-Domains A1
MVB	Munich Vascular Biobank
MYH11	Myosin Heavy Chain 11
MYH9	Myosin Heavy Chain 9
Mφ	Macrophage
NDM	Non-dilated of AAA With Enzymes of Milt Kit;
NDS	Non-dilated of AAA with Self-prepared Enzymes
NETs	Neutrophil Extracellular Traps
NFKBIA	NFKB Inhibitor Alpha
NR2F1	Nuclear Receptor Subfamily 2 Group F Member 1
OSR	Open Surgical Repair
PBS	Phosphate-Buffered Saline
PC	Plasma Cell
PECAM1	Platelet and Endothelial Cell Adhesion Molecule 1
PI16	Peptidase Inhibitor 16
POSTN	Periostin
PPE	Porcine Pancreatic Elastase
PS	Penicillin–Streptomycin
PTGS2	Prostaglandin-Endoperoxide Synthase 2
PTPRB	Protein Tyrosine Phosphatase Receptor Type B
PVAT	Perivascular Adipose Tissue
PVT1	Plasmacytoma Variant Translocation 1
RCIA	Right Common Iliac Artery
RHOB	Ras Homolog Family Member B

RNA-seq	RNA sequencing
RRA	Right Renal Artery
RT	Reverse Transcription
S100A8	S100 Calcium Binding Protein A8
SCD	Stearoyl-CoA Desaturase
SCN7A	Sodium Voltage-Gated Channel Alpha Subunit 7
scRNA-seq	Single Cell RNA-sequencing
SDPR	CAVIN2, Caveolae Associated Protein 2
SELENOP	Selenoprotein P
SEM	Stem Cell, Endothelial Cell, Monocyte
SERPINB9	Serpin Family B Member 9
SERPINE1	Serpin Family E Member 1
SFRP2	Secreted Frizzled Related Protein 2
STX8	Syntaxin 8
TAGLN	Transgelin
TC	T Cells
THY1	Thy-1 Cell Surface Antigen
TIMP	Tissue Inhibitors of Matrix Metalloproteases
TIMP1	Tissue Inhibitors of Matrix Metalloproteases 1
TNF	Tumor Necrosis Factor
TNFRSF11B	TNF Receptor Superfamily Member 11b
TREM2	Triggering Receptor Expressed on Myeloid Cells 2
TSPO	Translocator Protein
TUM	Technical University Munich
TXNIP	Thioredoxin Interacting Protein
UMAP	Uniform Manifold Approximation and Projection
UMI	Unique Molecular Identifier
VCAM1	Vascular Cell Adhesion Molecule 1
VCAN	Versican
VSMC	Vascular Smooth Muscle Cell
VWF	Von Willebrand Factor

LIST OF FIGURES

LIST OF TABLES

1. INTRODUCTION

1.1 Abdominal Aortic Aneurysm

1.1.1 Definition, Risk Factors and Complications

Abdominal aortic aneurysm (AAA) is defined as a permanent local dilation of the abdominal aortic diameter of more than 3cm or exceedingly more than 50% the size of the normal aorta (as shown in ***Figure 1***). Its prevalence increases along with age (Sampson et al., 2014) and is higher in developed countries than in developing countries (894 versus 685 per 100,000) among people aged ≥60.

Currently, risk factors for AAA are artificially classified into modifiable and non-modifiable. The former includes smoking, hypertension, atherosclerotic diseases, hypercholesterolemia, etc. The latter are represented by male gender, advanced age (≥60), family history (Eckstein and Maegdefessel, 2019). Interestingly, patients with diabetes mellitus, one of the common risk factors of cardiovascular diseases, hold a lower risk of developing AAA(Wanhainen et al., 2019).

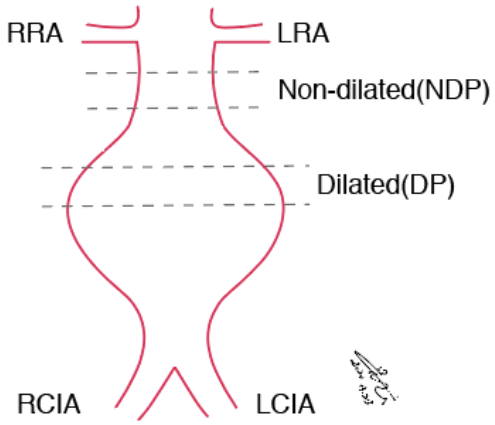

Figure 1. Abdominal aortic aneurysm (AAA). AAA is characterized as larger than 3 cm or exceedingly more than 50% the size of the normal aorta. Notes: NDP, non-dilated part of the AAA tissue; DP, dilated part of the AAA; RRA, right renal artery; LRA, left renal artery; RCIA, right common iliac artery; LCIA, left common iliac artery.

AAA usually remains asymptomatic until rupture or other relevant complications occur, i.e., distal artery emboli, aorto-enteric or aortocaval fistulae, etc. Although small AAAs can develop with different patterns (linear model (Newby et al., 2017), exponential type (Badger et al., 2011), or staccato pattern

(Vega de Céniga et al., 2008)), usually the higher the aneurysm size is, the higher is the rupture risk (Parkinson et al., 2015). One typical symptom is abdominal pain, indicating a possibility of rupture, which can threaten AAA patients life with an up to 80% mortality rate (Golledge, 2019). Routine imaging examinations like ultrasound, computed tomography (CT) are recommended for screening people with risk factors.

1.1.2 Clinical Prevention and Treatment

As previously mentioned, no AAA-specific pharmacological treatment is yet available and imaging-based routine screenings, as well as smoking cessation, remain the principal strategies for prevention/ monitoring AAA development and progression. Some clinical studies however investigated the efficacy in treating AAA of conventional drugs employed in treatment of cardiovascular diseases of different nature (i.e., telmisartan, (Golledge et al., 2020)), but none of them turned out to be effective in limiting the rate of aneurysm growth. Lipid-lowering therapy, beta-blockers, and anti-platelet drugs can be applied as "side strategies" to reduce patients' cardiovascular risks.

Surgical repair represents the current main approach to treat AAA. According to current guidelines, elective surgical repair is recommended when:(1) aneurysm maximal diameter is ≥5.5 cm for men or ≥5.0 cm for women; (2) aneurysm growth rate is faster than 1 cm per year; (3) AAA is accompanied by symptoms (Wanhainen et al., 2019). Open surgical repair (OSR) and endovascular aortic repair (EVAR) are the two main surgical procedures in today's clinical practice. OSR has been practiced since 1951 to reduce the burden of AAA (Dubost et al., 1951) and was not challenged until the 1990s when EVAR was firstly introduced (Parodi et al., 1991). Although the goals of OSR and EVAR are the same, debates about the pros and cons of both methodologies have never stopped since the emergence of EVAR. While OSR poses trauma and high perioperative risks, routine EVAR requires suitable anatomical conditions to achieve the ideal treatment effect. Recent clinical trials and meta-analysis indicated that EVAR showed advantages

over OSR during the perioperative period (Lederle et al., 2012; Patel et al., 2016; Powell et al., 2017; Chen et al., 2019). Moreover, advanced endovascular techniques (i.e., fenestrated/ branched grafts (Marzelle et al., 2015; Makaloski et al., 2018), chimney/sandwich techniques (Wu et al., 2017; Wu et al., 2019a)) can also be applied to complex AAAs to achieve better prognosis and to avoid surgical trauma. However, except for yet known complications (i.e., endoleaks, occlusions, etc.) in EVAR, patients may also undergo catastrophic complications, like aortic intimal intussusception (Wu et al., 2019b). In the long term, patients under EVAR may suffer more re-interventions than those with OSR (Chen et al., 2019).

1.1.3 Biological View on Development and Progression of AAA

Although our understanding of AAA pathogenesis is rapidly accelerating, many issues remain to be elucidated on the path towards development of effective therapeutic strategies. In this context, *in vivo* and *in vitro* studies can provide us with deep insights into the AAA development and progression. AAA animal models (Lysgaard Poulsen et al., 2016) include mouse models (Angiotensin II hypercholesterolaemic knockout model, elastase model, calcium chloride model), rat models and porcine models. As each animal model has its pros and cons; the employment of multiple animal models is useful to approach the study of AAA from different perspectives.

Based on *in vitro* studies of human AAA tissues obtained from OSR, the culprit lesions are orchestrated by all layers of the aortic wall (Maegdefessel et al., 2013), including endothelial cells (ECs), immune cells (monocytes, T cells, B cells, macrophages, dendritic cells, etc.), vascular smooth muscle cells (VSMCs) and adventitial cells (Wu et al., 2020). Scientific reports focusing on these cell types have extensively contributed to the development of current theories on AAA pathogenesis, which mainly include atherothrombosis, inflammation and inherited factors (Golledge, 2019).

One important contributor to AAA pathogenesis are VSMCs, constituting the main component of the aortic wall and residing in the medial aortic layer. VSMCs

can modulate vasoconstriction and vasodilatation, playing a contractile function under non-diseased conditions; it can also express extracellular matrix(ECMs), tissue inhibitors of matrix metalloproteases (TIMPs) (Wilson, 2011). However, if stimulated by local factors like inflammatory cytokines, oxidized lipids, vessel wall injury, etc., VSMCs can undergo apoptosis and switch from a contractile to a synthetic phenotype (Ailawadi et al., 2009; Wilson, 2011; Wu et al., 2020). VSMC apoptosis can be induced during vascular disease development by NETosis (Silvestre-Roig et al., 2019), a program induced cell death mechanism, which is triggered by neutrophil extracellular traps (NETs). Whether this mechanism contributes to AAA needs to be further elucidated (Plana et al., 2020). Conversely, perivascular adipose tissue (PVAT) was recently found to play a vital role in AAA (Cheng et al., 2018; Dias-Neto et al., 2018; Kugo et al., 2019; Sagan et al., 2019), with more mechanistic studies being still required.

Beyond the cellular level, researchers in this field have extended the theories of AAA formation to the transcription level i.e. noncoding RNAs (ncRNAs) which aren't finally translated into proteins. NcRNAs encompass a wide range of categories including microRNAs, long noncoding RNAs(lncRNAs), etc. MicroRNAs have been well studied (Kumar et al., 2019; Wu et al., 2020) and several functional lncRNAs like H19 (Li et al., 2018; Zhang et al., 2018), PVT1 (Zhang et al., 2019b) have also been demonstrated a quite critical role in AAA, as summarized in two recent reviews (Kumar et al., 2019; Wu et al., 2020). Among these ncRNA studies, aortic tissues from human or animal models are usually harvested and sent for bulk RNA sequencing to detect differentially expressed genes (DEGs), or to perform other analysis between healthy and diseased tissue specimens, and finally to get these ncRNAs of interest.

1.2 Single-Cell RNA Sequencing

Since the new millennium, novel platforms, known as Next Generation Sequencing (NGS), have marked the rise of the genomic era. Cutting edge technologies nowadays allow to determine nucleic acid sequences with extreme accuracy at

unprecedented scale. In particular, transcriptomic analysis have contributed to investigate the mechanism of gene expression regulation and to unveil the central role of RNA in orchestrating this previously underestimated complexity. A wide variety of RNA sequencing (RNA-seq) techniques has been developed and continuously improved, which can be preferentially employed upon specific technical needs required to address desired biological questions (Lagarde et al., 2017; Sahraeian et al., 2017; Garalde et al., 2018).

Transcriptomic analysis are usually employed to profile average DEG patterns, upon different conditions (healthy vs disease, treatment vs control, etc.), starting from bulk tissue samples (Chaudhry et al., 2019). However, when investigating the contribution to disease of a specific cell type or population, one technique that goes beyond bulk sequencing is the single cell RNA-sequencing (scRNA-seq), which can discern DEGs at single-cell level (Stark et al., 2019). ScRNA-seq techniques allow indeed to reveal potential cellular heterogeneity or phenotypic plasticity (van Kuijk et al., 2019).

Since the advent of the first scRNA-seq methodologies in 2009 (Lao et al., 2009; Tang et al., 2009), huge advances have been achieved and novel approaches have been introduced. In the following sections, the three main scRNA-seq platforms currently available and examples of their applications in the field of vascular biology will be introduced.

1.2.1 Three Main scRNA-seq Methodologies

The three main scRNA-seq methodologies to profile DEGs at single cell level, with different throughputs, ranging from a few to thousands or even millions of cells, include microtiter-plate-based, microfluidic systems-based and split-pool barcoding-based approaches (Lafzi et al., 2018).

(1) Microtiter plates.

With this method single cells can be sorted into a 96- or 384-well format microtiter-plate and selected by Fluorescence Assisted Cell Sorting (FACS) system.

An example of widely used method is represented by Smart-seq2 (Picelli et al., 2014). Despite high accuracy and sensitivity, Smart-seq2 only harvest few cells (Ziegenhain et al., 2017). Sensitivity improvements have recently been made (Smart-seq3, (Hagemann-Jensen et al., 2019)). Furthermore, Smart-3SEQ (Foley et al., 2019), single cell partitioning is achieved by laser-capture microdissection. Smart-3SEQ should be preferred for samples with limited number of cells, like formalin-fixed paraffin-embedded (FFPE) tissues. The overall costs of the Smart-seq platform are high.

Other methods based on a plate can be referred to STRT-seq (Islam et al., 2012), SCRB-seq (Soumillon et al., 2014), msSCRB-seq (Bagnoli et al., 2018), CEL-seq (Hashimshony et al., 2012), CEL-seq2 (Hashimshony et al., 2016), Quartz-seq (Sasagawa et al., 2013), Quartz-seq2 (Sasagawa et al., 2018), MARS-seq (Jaitin et al., 2014), as also shown in ***Figure 2***.

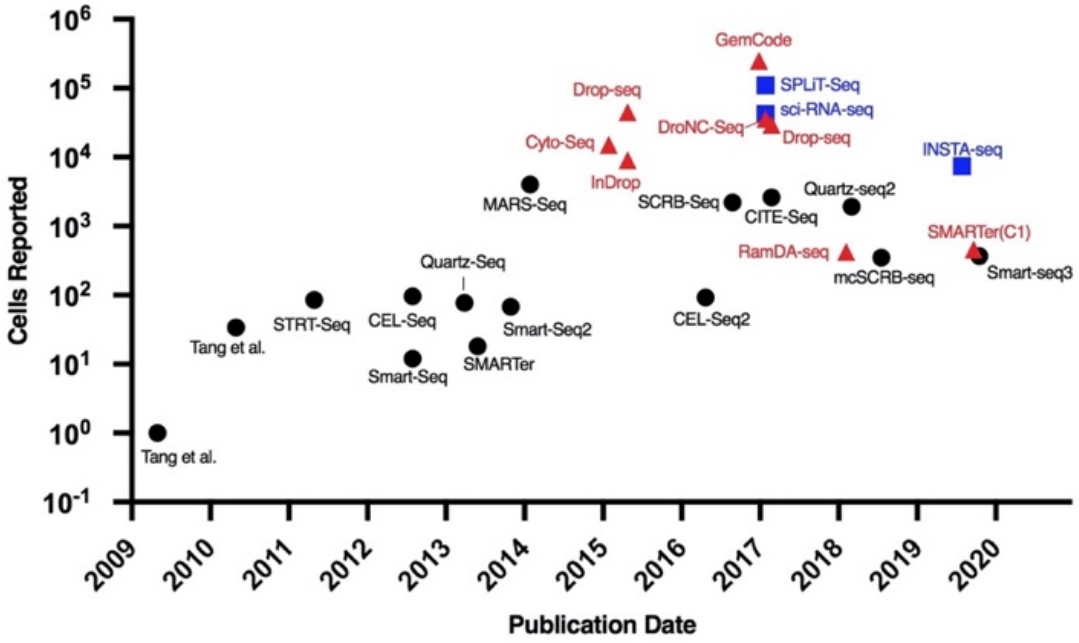

Figure 2. A Brief history of the single-cell RNA sequencing. Cell numbers reported in some representative scRNA-seq methods by publication date, adapted and updated from (Hashimshony et al., 2016; Bagnoli et al., 2018; Hayashi et al., 2018; Sasagawa et al., 2018; Svensson et al., 2018; Fürth et al., 2019; Hagemann-Jensen et al., 2019; Verboom et al., 2019). The red triangles indicate techniques based on microfluidic systems. The black circles indicate techniques based on microtiter plate-partitioning. The blue boxes indicate techniques based on *in situ* barcoding.

(2) Microfluidic systems.

Compared to the microtiter-plate-based approach, microfluidic-based scRNA-seq approaches allow higher throughput (thousands of cells) at relatively lower costs. Different droplets-, nanowells- and integrated fluidics circuits-based systems have been developed to capture and split cells. Among the droplets-based system, droplet-based partitioning can be achieved by taking advantage of Drop-seq (Macosko et al., 2015), inDrop (Klein et al., 2015) and Chromium 10X (Zheng et al., 2017) platforms. The workflows of droplets-based platforms are quite similar and include five main steps: 1)single-cell suspension preparation, 2)droplet encapsulation, 3)cDNA synthesis and amplification, 4)sequencing and 5) computational analysis (Salomon et al., 2019). In particular, in the Chromium 10X platform, a "water-in-oil" or Gel Bead-In-Emulsions (GEM, ***Figure 3***) is generated, which ideally includes a single cell, a gel bead with barcoded reverse transcription (RT) primers, enzymes and partitioning oil. As shown in ***Figure 3***, the 10X barcodes are specific for identifying RNA molecules belonging to the same cell during the later computational multiplexing process. The UMIs are molecular barcodes for labeling and quantifying unique RNA molecules. However, one possible drawback is the possibility for a "water-in-oil" to contain more than one cell.

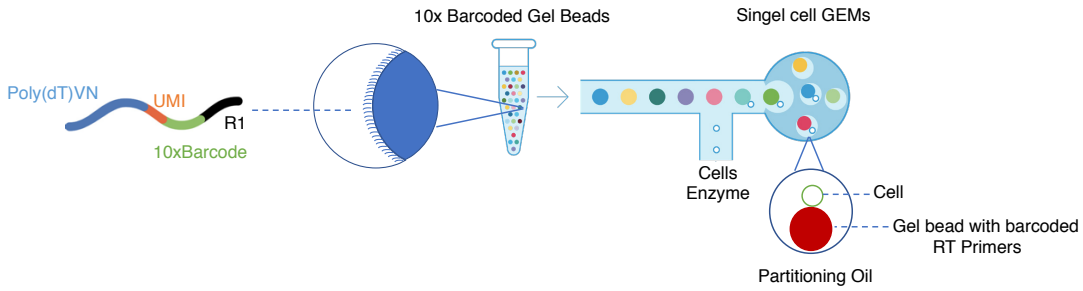

Figure 3. Single cell Gel Bead-In-Emulsions (GEM) in Chromium 10X platform. (Adapted from *Chromium Next GEM Single Cell 3' Reagent Kits v3.1*(CG000204 Rev D)).

Principles or details about the other two microfluidic system-based approaches could refer to Drop-seq[41] and inDrop[42] (***Figure 2***), as well as other literature (Ziegenhain et al., 2017; Wang et al., 2019). One additional

interesting method may be the recent SMARTer system that claims the capacities of detecting circular RNAs (Verboom et al., 2019).

(3) *In situ* barcoding

Conversely to the two previously described approaches, with *in situ* barcoding-based methods (also called split-pool barcoding) cells are pooled and redistributed into 96- or 384-well plates and subsequently barcodes are applied (i.e. sci-RNA-seq, (Cao et al., 2017); SPLiT-seq (Rosenberg et al., 2018); INSTA-seq (Fürth et al., 2019)). While barcoding is achieved in only one step with the Chromium 10X platform, this takes several rounds when using *in situ* barcoding technologies. The most appealing features are their throughput (thousands to millions of cells), as well as the costs per cell, which are much lower compared to the two prior approaches. Furthermore, cells are fixed on a plate, which can be stored for further experiments.

1.2.2 Applications of scRNA-seq in Vascular Disease

ScRNA-seq has been extensively performed and are shaping our understanding on the mechanisms of cardiovascular diseases (Chaudhry et al., 2019). It has also been adopted to study physiological aspects of vascular development and differentiation, as well as to investigate vascular disease pathogenesis (Chavkin and Hirschi, 2020).

Thanks to this technology, the transcriptional landscape of mouse vascular system at single-cell level has been made available to the scientific community (Kaur et al., 2017; Dobnikar et al., 2018; Kalluri et al., 2019). A pioneer study focused on the heterogeneity of G-protein-coupled receptor in the vascular system, pointing out the existence of a population of spontaneously dedifferentiating VSMC in the healthy aorta (Kaur et al., 2017). Dobnikar and colleagues (Dobnikar et al., 2018) demonstrated the VSMC heterogeneity in vascular beds and proved the capability of a multipotent progenitor marker, Sca1, in regulating VSMC phenotypic switching by downregulating contractile genes and upregulating

synthetic genes. They further found a population of Sca1-positive VSMC in murine atherosclerotic plaques (Dobnikar et al., 2018). Another recent study (Kalluri et al., 2019) revealed three EC subpopulations in the mouse aorta as characterized by distinct functional roles.

ScRNA-seq was also applied to profile different cell populations characterizing human atherosclerotic plaques(Fernandez et al., 2019). In particular, different T cells and macrophages phenotypes were identified in plaques, blood and vascular tissue from symptomatic versus asymptomatic patients (Fernandez et al., 2019). However, differences in cell composition between stable and unstable plaques still remains unexplored. In PVAT, mesenchymal stem cells (MSCs) were found of heterogeneity in two subpopulations, contributing to vascular remodeling and VSMC differentiation (Gu et al., 2019).

In the context of aortic aneurysm, scRNA-seq analysis have been carried out in a human thoracic aorta study (Pedroza et al., 2020) and a murine abdominal aorta study (Zhao et al., 2020). However, no scRNA-seq-based studies focusing on human AAA has yet been introduced.

2. AIMs

This study aims at exploiting scRNA-seq to obtain novel biological insights into AAA disease. Detailed aims are:

(1) To set up a pipeline for the analysis of AAA scRNA-seq data and to compare single cell expression patterns in the non-dilated versus the dilated portion of human AAA tissue collected from open repair surgeries.

(2) To identify expression profiles of immune cells and structural cells at single-cell level.

(3) To explore cellular heterogeneity in human AAA disease.

3. MATERIALS AND METHODS

This study was approved by the local ethics committee and was conducted in line with the ethical guidelines of Technische Universität München, Klinikum rechts der Isar. The investigation of human samples here conformed with the principles of Declaration of Helsinki (Helsinki, 1997).

3.1 Patient Sample Source

Human AAA samples utilized in this study were obtained from the *Munich Vascular Biobank (MVB)* (Pelisek et al., 2019). A written informed consent form was signed by all patients. This study was approved by the Ethics Committee of Technische Universität München, Klinikum rechts der Isar (Project number: 2799/10).

3.2 Workflow

As shown in ***Figure 4***, the workflow for AAA scRNA-seq carried out in this study mainly includes five steps:

(1) AAA tissue collection from patients undergoing elective OSR;
(2) Aortic dissociation *via* mechanical mincing and enzymatic digestion;
(3) Micro-fluidic system-based scRNA-seq library preparation (10x Genomics Chromium Platform);
(4) Single cell RNA sequencing (Illumine NovaSeq6000);
(5) *In silico* analysis (R package).

In detail, the more upstream non-dilated neck was dissected and separated from the downstream dilated portion of the AAA, as shown in ***Figure 1*** *and* ***Figure 4***. Both tissue fragments subsequently underwent enzymatic digestion, according to two alternative dissociation protocols, which were applied to each aortic portion in parallel (an "in-house-developed" procedure referred to as "Self" versus a commercial kit, labeled "Milt"). Thus, four samples were eventually submitted to sequencing analysis ("Dilated_Self"; "Non-dilated_Self"; "Dilated_Milt"; "Non-

dilated_Milt"). Details about the two applied digestion protocols will be introduced in the following section (*3.3 Aortic Dissociation*).

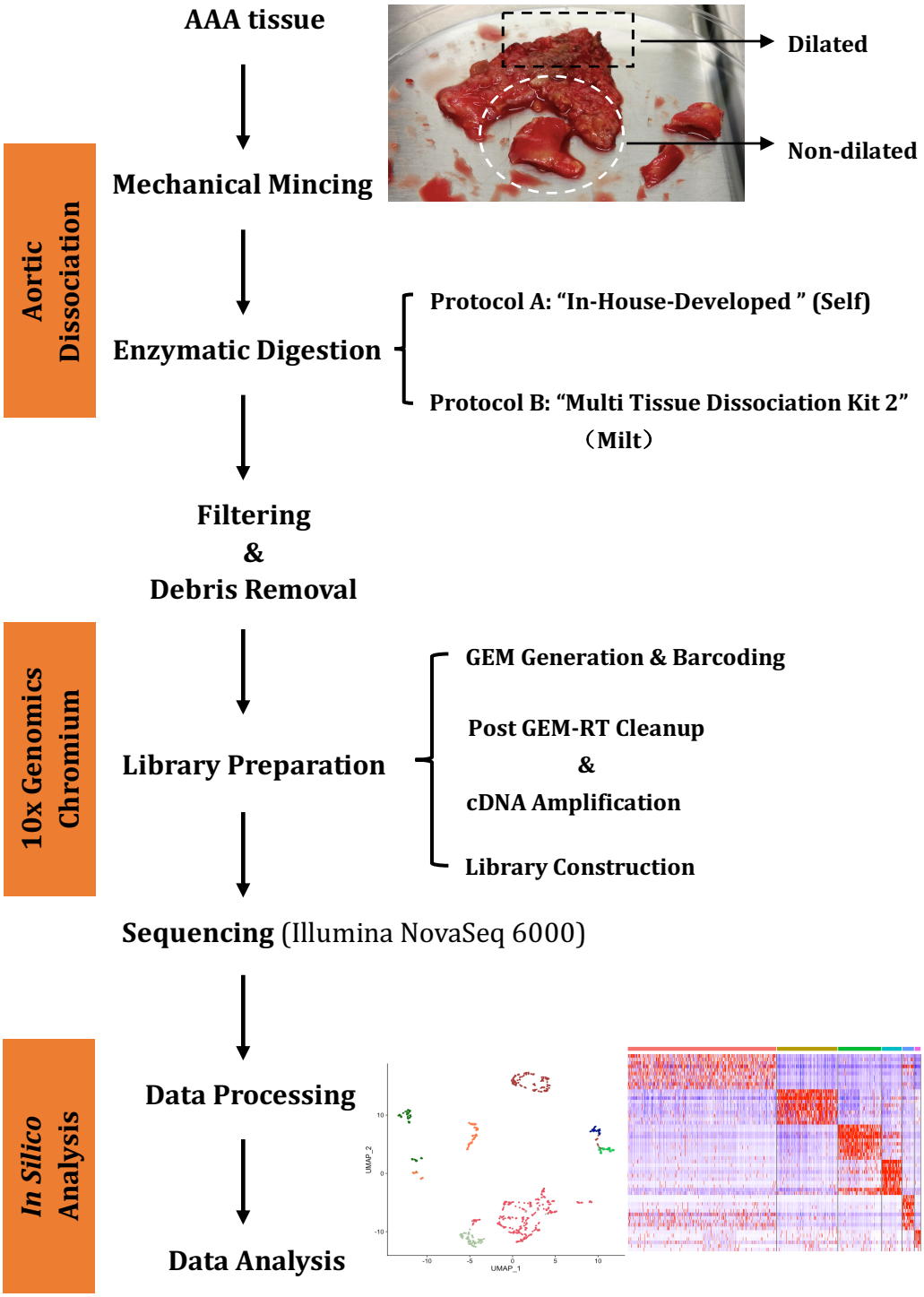

Figure 4. Workflow of the experiment. Samples obtained from the operative room were promptly transferred to the cell culture lab for mechanical and enzymatic dissociation. Sequencing libraries were prepared according to 10X Genomics Chromium Platform, sequenced with Illumina NovaSeq6000 system and analyzed *in silico*. Notes: GEM, gel bead-in-emulsions.

3.3 Aortic Dissociation

AAA tissue samples obtained from patients undergoing elective OSR were promptly placed in phosphate-buffered saline (PBS, Sigma Aldrich, Lot# RNBJ1283) and transferred on ice to the cell culture lab. Samples were processed within one hour after surgery. After rinsing in PBS to wash any blood or thrombus residues, the non-dilated neck was dissected and separated from the dilated aneurysmal fragment, for subsequent dissociation procedures. Two alternative enzymatic digestion protocols were compared: an "in-house-developed" enzymatic cocktail, referred to as "Self" (0.8 mg/ml Collagenase A; 2.68 Kunitz/ml DNase l in DMEM/F12 Medium (Dulbecco's Modified Eagle's Medium/Nutrient Mixture F-12 Ham; Sigma Aldrich, Lot# RNBH2773) with 5% FBS(Fetal Bovine Serum) and 1% penicillin–streptomycin (PS)), and a commercial kit "Multi Tissue Dissociation Kit 2" (Miltenyi Biotech, 130-110-203), referred to as "Milt". Both dissociation process lasted about 1 hour. Details of the procedures for aortic dissociation relative to each protocol follow:

(1) Materials

1) Scalpel, forceps and 1ml Syringe,
2) Two to three cell culture dishes,
3) Cell Strainer 70 μm (EASYstrainer™, Cat. -no.542070),
4) Cell Strainer 40 μm (EASYstrainer™, Cat. -no.542040),
5) PBS (Sigma Aldrich, Lot# RNBJ1283) at room temperature,
6) PBS (Sigma Aldrich, Lot# RNBJ1283) at 4 °C,
7) Trypan Blue solution (Sigma Aldrich, Lot# RNBH2126)
8) DMEM-F12 +10% FBS + 1% PS,
9) Multi Tissue Dissociation Kit 2 (Miltenyi Biotech, 130-110-203),
10) GentleMACS C Tube (Milteny Biotech, 130-096-334),
11) GentleMACS Dissociator (Miltenyi Biotech, 130-093-235),
12) Debris Removal Solution (Miltenyi Biotech, 130-109-398).

(2) Protocol

1) Obtain vessel biopsy and wash with sterile PBS. Cut with a sharp sterile scalpel into small pieces.
2) For commercial enzyme kit: Add 2.3 mL of Buffer X, 62.5 µL of Enzyme P, 25µL of Buffer Y,100µL of Enzyme D and 12.5µL of Enzyme A of the Multi Tissue Dissociation Kit 2 into a GentleMACS C Tube. Prepare the same volume of the enzyme from homemade protocol as mentioned above into another GentleMACS C Tube.
3) Transfer biopsy pieces into a GentleMACS C Tube containing the enzyme mix and tightly close C Tube and attach it upside down onto the sleeve of the GentleMACS Dissociator.
4) Run the GentleMACS Program “37C_Multi_G”.
5) After termination of the program, detach “C Tube” from the GentleMACS Dissociator.
6) Apply the cell suspension to a 70 µm strainer placed in a petri dish.
7) Add 7 mL of cell culture medium with FBS into the C Tube to collect leftover cells. Strain the cells through the filter with the inlay of a 1ml syringe.
8) Strain the cell suspension through another strainer (40 µm) placed on a 50 mL tube.
9) Centrifuge cell suspension at 300×g for 5 minutes, 4°C.
   From now on, stay at 4°C!
10) Carefully suction off the medium, be careful not to disturb the cell pellet.
11) Resuspend in 3,1 mL of cold PBS and transfer the cells in a 15 ml tube.
12) Add 900 µl Debris Removal Solution (Miltenyi Biotech) and mix well by slowly pipetting up and down several times.
13) Overlay the mix very gently with 4 ml cold PBS (Note: Trypan blue can be added for better visualization).
14) Centrifuge at 3000×g for 10 minutes, 4°C.
15) Aspirate the two top phases completely and discard them.

16) Full up with cold PBS to a final volume of 15 ml.
17) Mix by gently inverting the tube 3 times.
18) Centrifuge at 1000×g for 10 minutes, 4°C.
19) Aspirate supernatant completely and resuspend in 1-2 ml cold PBS.
20) Place in the fridge or on ice until counting.
21) Count the cells and prepare the cell suspensions with target concentrations according to the instructions of *Chromium Next GEM Single Cell 3' Reagent Kits v3.1*(CG000204 Rev D).

3.4 Single-cell RNA Library Preparation and Sequencing

ScRNA-seq libraries preparation and cDNA synthesis were carried out according to 10x Genomics Chromium Platform (Zheng et al., 2017; Azizi et al., 2018), following manufacturer's instructions (CG000204 Rev D). In particular, libraries were constructed with P5, TruSeq Read 1 (sequencing primer site), 16bp 10x Barcode (for identifying cells), 12bp UMI (for identifying molecules), TruSeq Read 2(sequencing primer site), Sample Index (for indexing sample), P7. Sequencing was performed by taking advantage of Illumina NovaSeq 6000 Sequencing system.

3.5 Demultiplexing

Raw data obtained from sequencing was demultiplexed according to 10x Genomics pipeline by using Cell Ranger v2.1.0 software (https://support.10xgenomics.com). A gene-barcode matrix was generated for each library, and cell barcodes and UMIs were corrected and filtered.

3.6 Single-Cell Data Analysis

R package Seurat (version 3.1.4) (Butler et al., 2018; Hafemeister and Satija, 2019; Stuart et al., 2019) was used for analysis of scRNA-seq data in RStudio (version 1.2.5001). For each Seurat object created, genes were filtered out if expressed in fewer than 5 cells. Moreover, during preprocessing, two further filtering conditions were set:

(1) Maximum of 3000 genes and minimum of 100 genes were expressed per cell;

(2) Mitochondrial genes more than 20% of the expressed genes in the cell.

Possible confounding factors arising from cell cycle heterogeneity were mitigated by using the CellCycleScoring function(Barron and Li, 2016). SCTransform normalization in Seurat was also applied to remove technically driven, as well as other sources of variations (Hafemeister and Satija, 2019). Principal component analysis (PCA) was run (RunPCA function) for further dimensional reduction and unsupervised cell clustering. The Uniform Manifold Approximation and Projection (UMAP) was used to convert cells into a two-dimensional map (dimension of reduction set at 1:20).

Clustering was performed with Seurat FindClusters function, with a resolution of 0.1 in order to get the main cell types. Labeling of clusters with cell-type identities was achieved by using Enrichr (*https://amp.pharm.mssm.edu/Enrichr/*) (Chen et al., 2013; Kuleshov et al., 2016), as well as by referring to canonical markers. Sub-clustering was further obtained raising the resolution in FindClusters function. All markers were tabled with the FindAllmarkers function. Gene Ontology(GO) analysis comparison, KEGG pathway, and Reactome Pathway Enrichment comparison (Yu et al., 2012; Yu and He, 2016) were also applied for related analysis with top-expressed markers. Differentially expressed genes (DEGs) were detected by utilizing FindAllmarkers function in Seurat, with default statistical method. An adjusted P value of 0.05 was considered as the threshold of statistical significance.

3.7 Statistical Analysis

RStudio (version 1.2.5001) was used for the statistical analysis. Marker genes of each cluster were identified by using FindAllmarkers function of Seurat package, by applying default Wilcoxon rank-sum statistics. Other statistical methods used in this manuscript were applied with default settings, unless differently specified. Prism 8 (Version 8.2.1, GraphPad Software) was utilized for data representation.

3.8 Data Availability

All the data and methods described in this manuscript are available upon request to the Vascular Biology and Experimental Vascular Medicine Unit, Department of Vascular and Endovascular Surgery of the Technical University Munich (TUM) (contact@vascular-tum.de or https://www.vascular-tum.de/).

4. RESULTS

4.1 Single-cell RNA Profiling and Unbiased Clustering of Human Abdominal Aneurysmal Aorta

The specimens were finally prepared from two sites (dilated part and non-dilated aortic neck) of the AAA collected from one patient undergoing elective OSR (***Figure 1***). Two dissociation protocols were applied in parallel on both the dilated and the non-dilated aortic fragments, thus ending up with 4 different samples (labeled "Dilated_Self"; "Non-dilated_Self"; "Dilated_Milt"; "Non-dilated_Milt", details seen in Methods section). Single-cell suspensions and the final libraries for sequencing were prepared according to the instructions of 10X Genomics Chromium Platform. The sequencing dataset was then processed with Cell Ranger (also described in the Methods) and was subsequently analyzed.

A total of 1690 cells were finally harvested from the four sequenced samples. Detailed descriptions about the estimation of the cell-barcode and UMIs in each library are listed in ***Table S1***, as well as the number of cells from each sample. Noteworthy, the use of different enzymatic digestion protocols did not affect the enrichment of any specific cell type, as shown in ***Figure 5A***. Furthermore, cell populations did not significantly differ between non-dilated and dilated tissue samples (***Figure 5B***). Similar features in terms of cell type could also be observed among the four sequenced samples (***Figure 5C***). Based on these observations and as a consequence of the limited number of sequenced cells within each sample, data relative to each group were merged together for subsequent analysis.

After processing with the filtering conditions, 983 cells were included in further analysis steps. Unbiased clustering identified 15 distinct subpopulations (***Figure 5D***), including monocytes/macrophages (Mono/Mφ, cluster 0, 1, 2, 3, 9 and 13), T cells (cluster 4, 7), B cells(cluster 11) and plasma cells (cluster 5), ECs (cluster 10, 14), VSMCs (cluster 8) and adventitial cells (cluster 6, 12). The top ten markers of each cluster are depicted in ***Figure 5E*** and ***Table S2***.

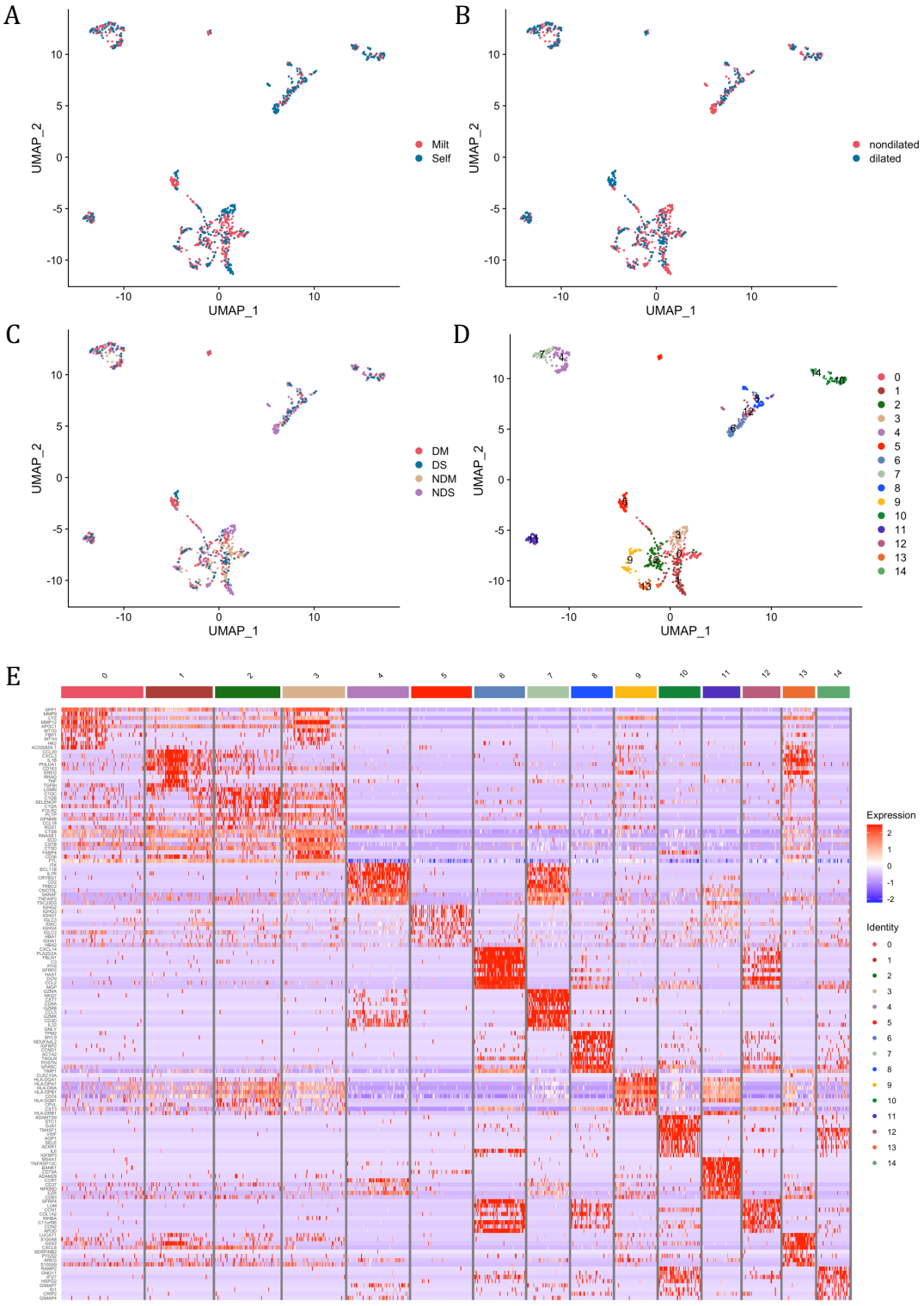

Figure 5. Cell populations in AAA identified by ScRNA-seq analysis. A. Cell clusters from two different dissociation protocols are not significantly different; B. Cell clusters from non-dilated and dilated AAA are not significantly different; C. Cell cluster identified in the four libraries (DS, NDS, DM, NDM) are not significantly different. D. scRNA-seq identified 15 distinct clusters; E. Top ten markers for each cluster (weighed by avg_logFC) of each cluster. Notes: DM, Dilated_Milt group; DS, Dilated_Self group; NDM, Non-dilated_Milt group; NDS, Non-dilated_Self group.

4.2 Cell Amount and Percentage Altered in Dilated AAA Compared to Non-dilated Aortic Neck

Next, the proportion of each cell type was calculated. Among the cells after processing, immune cells accounted for 73.04% (718/983) including macrophages, monocytes, dendritic cells, T cells, and B cells (***Figure 6A,*** *left and middle*). Among these immune cells, macrophages represented the largest population (50.14%, 360/718), followed by T cells 13.63% (134/983), B cells for 4.98% (49/983) and monocytes accounted for 4.4% (54/983). On the other hand, structural cells (26.96%, 263/983) mainly included adventitial cells, VSMCs, and ECs, which were respectively 11.70% (115/983), 5.49% (54/983) and 9.77% (96/983), as shown in ***Figure 6A*** and ***Table 1***.

In order to explore differences in the amount of cells populating each cluster in dilated *versus* non-dilated AAA, the percentage of each cell type per cluster was calculated and compared. Interestingly, the greater proportion of cells 61.85% (608/983) came from non-dilated fragment, likely due to consistent apoptosis and subsequent reduced cell number characterizing the aneurysmal dilated region. At the same time, in line with results from a AAA mouse study (Zhao et al., 2020), the fraction of immune cells, significantly increased at the site of aneurysm, as shown in ***Figure 6B*** (T cells, non-dilated: 10.69%, 65/608 *vs* dilated: 18.40%, 69/375; B cells, non-dilated: 3.45%, 21/608 *vs* dilated: 7.47%, 28/375.). However, this was not true for macrophages, depleted in dilated part (30.40%, 114/375).

As regards structural cells, the percentage of fibroblasts in the non-dilated fragment (14.47%, 88/608) was remarkably reduced in dilated AAA (7.2%, 27/375), as shown in ***Figure 6B*** *and* ***Table 1***. On the contrary, the number of VSMCs and ECs were similar between the two groups.

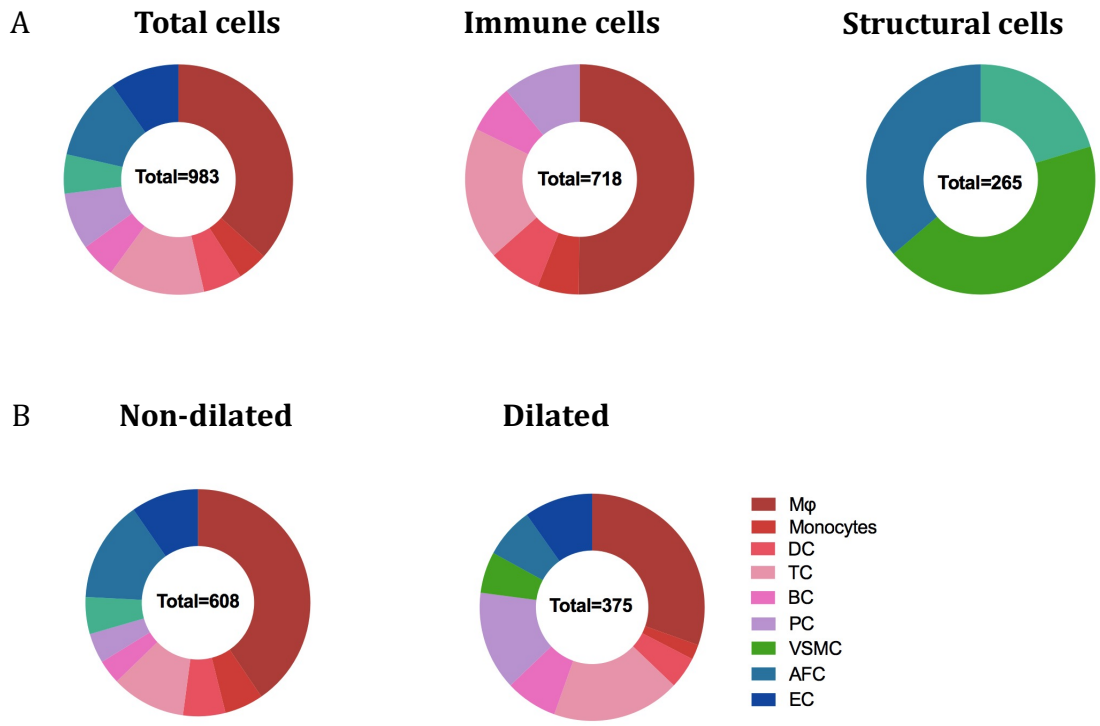

Figure 6. Proportions of main cell types. A. Cell composition of total cells (dilated + non-dilated, left), immune cells (middle) and structural cells (right); B. Comparison between cell composition in non-dilated dilated AAA. Notes: Mφ, macrophages; DC, dendritic cells; TC, T cells; BC, B cells; PC, plasma cells; VSMC, vascular smooth muscle cell; AFC, adventitial cells; EC, endothelial cells.

Table 1. Cell amount and proportion of each cell type

	NDP (%)	DP (%)	Sum (%)	Total (%)
Mφ	246(40.46)	114(30.40)	360(36.62)	718(73.04)
Mono	34(5.59)	8(2.13)	42(4.40)	
DC	37(6.09)	17(4.53)	54(5.49)	
TC	65(10.69)	69(18.4)	134(13.63)	
BC	21(3.45)	28(7.47)	49(4.98)	
PC	26(4.28)	53(14.1)	79(8.03)	
VSMC	32(5.26)	22(5.87)	54(5.49)	265(26.96)
AFC	88(14.47)	27(7.2)	115(11.70)	
EC	59(9.70)	37(9.87)	96(9.77)	
Total	608(61.85)	375(38.15)	983	983

Notes: NDP, non-dilated part; DP, dilate part; Mφ, macrophages; Mono, monocytes; DC, dendritic cells; TC, T cells; BC, B cells; PC, plasma cells; VSMC, vascular smooth muscle cell; AFC, adventitial cells; EC, endothelial cells.

4.3 Heterogeneity of Monocytes/macrophages in Human AAA

Unsupervised clustering identified 6 distinct clusters of Mono/Mφ, assigned by referring to canonical markers LGALS3, CD68, CD14, FCGR3A (All the full names of gene abbreviations are listed in *Appendix*), as shown in ***Figure 7A***. Each cluster was then submitted to further analysis to better explore its specific features (***Figure 7B***). To this end, Seurat function FindAllmarkers was applied and the resulting top20 significantly DEGs (weighted by avg_log FC, p_val_adj<0.05) were presented in the heatmap, ***Figure7C*** and ***Table S3***. Based on the profiled signatures of each cluster, cluster labelling was assigned as follows: fibroblast-like Mφ (cluster 0), inflammatory-like Mφ (cluster 1), resident-like Mφ (cluster 2), foamy Mφ (cluster 3), Mo/DC (cluster9), and monocyte (cluster 13). Representative markers are shown in ***Figure 7D.*** GO enrichment comparison among all the six clusters are listed in ***Figure 7E***, as well as KEGG and Ractome pathway (***Figure 7F-G***).

"Fibroblast-like Mφ"(cluster0) signature genes like FN1 (Murphy and Hynes, 2014), MMP9, COL6A1 and COL6A2 (***Figure 7D***), play a crucial role in aneurysm formation, as involved in regulation of production of the extracellular matrix (ECM). Linked GO-terms were indeed "extracellular matrix structural constituent" and "collagen binding" (***Figure 7E***). "Inflammatory-like Mφ" (cluster 1) exhibited high expression of pro-inflammatory genes encoding for cytokines (TNF, IL1B, CCL20, CCL4, et al.) and chemokines (CXCL3, CXCL5, CXCL2; ***Figure 7D***). In agreement with a previous study (Cochain et al., 2018), the expression of inhibitors of NFκB signaling, like NFKBIA and IER3 (Schott et al., 2014), was also to be found in this cluster. Based on the expression of F13A1, FOLR2 and SELENOP (Willemsen and de Winther, 2020), cluster 2 was labeled as "resident-like Mφ". This included cells involved in antigen presentation, as inferred by the expression of genes encoding for complement proteins (C1QC, C1QB and C1QA, ***Figure 7D***), as long as Major Histocompatibility Complex Class II molecules (MHC class II, CD74, HLA-DPA1 and HLA-DPB1, ***Figure 7D***). Cluster 3 included "foamy Mφ", involved in cholesterol metabolism and PPARγ pathway signaling (FABP4 (Liu et

al., 2020), CD36 (Lamas Bervejillo et al., 2020), SCD), and sharing functional similarities with TREM2^{hi} Mφ (Cochain et al., 2018; Willemsen and de Winther, 2020). Cells belonging to this cluster presented increased expression of ECM-related genes like MMP12, MMP19, MMP14, as well as higher levels of cathepsins (CTSB, CTSZ, CTSD).

Cluster 9 was enriched in genes responsible for antigen processing and presentation (HLA-DQA1, CLEC10A (Hoober et al., 2019), HLA-DQB1, HLA-DRA, HLA-DPA1, HLA-DRB1) and thus labelled as "dendritic cells" (DC, ***Figure 7E***). Finally, cluster 13 expression profile (***Figure 7D***) was compatible with "monocytes" and included inflammation markers (S100A8 (Wang et al., 2018), PTGS2 (Rodemerk et al., 2020), IL1B, SERPINB9, CXCL8), along with ECM remodeling ones (VCAN, TIMP1) and ligands of epidermal growth factor receptor (AREG, EREG). Details about the pathway can also be found in ***Figure 7E***-G.

Macrophage clusters (cluster 0, 1, 2, and 3) accounted for 36.62% of the total cells, in particular 40.46% of the cells from the non-dilated fragment and 30.40% of cells from the dilated AAA, as shown in ***Table 1***. Differences in the relative percentage of each cluster in non-dilated versus dilated specimens are shown in ***Figure 7H***. In detail, the percentage of cluster 1 (inflammatory-like Mφ) and cluster 2 (resident-like Mφ) did not significantly vary (around 9% in both samples). Conversely, significant shifts occurred in cluster 0 (fibroblast-like Mφ) and cluster 3 (foamy Mφ), which dropped from 13%, to 7.47%, and from 10% to 5.33%, respectively, in dilated AAA. Similarly, the percentages of monocytes (cluster 13) and DCs (cluster 9) were also diminished in dilated AAA, compared to the non-dilated portion.

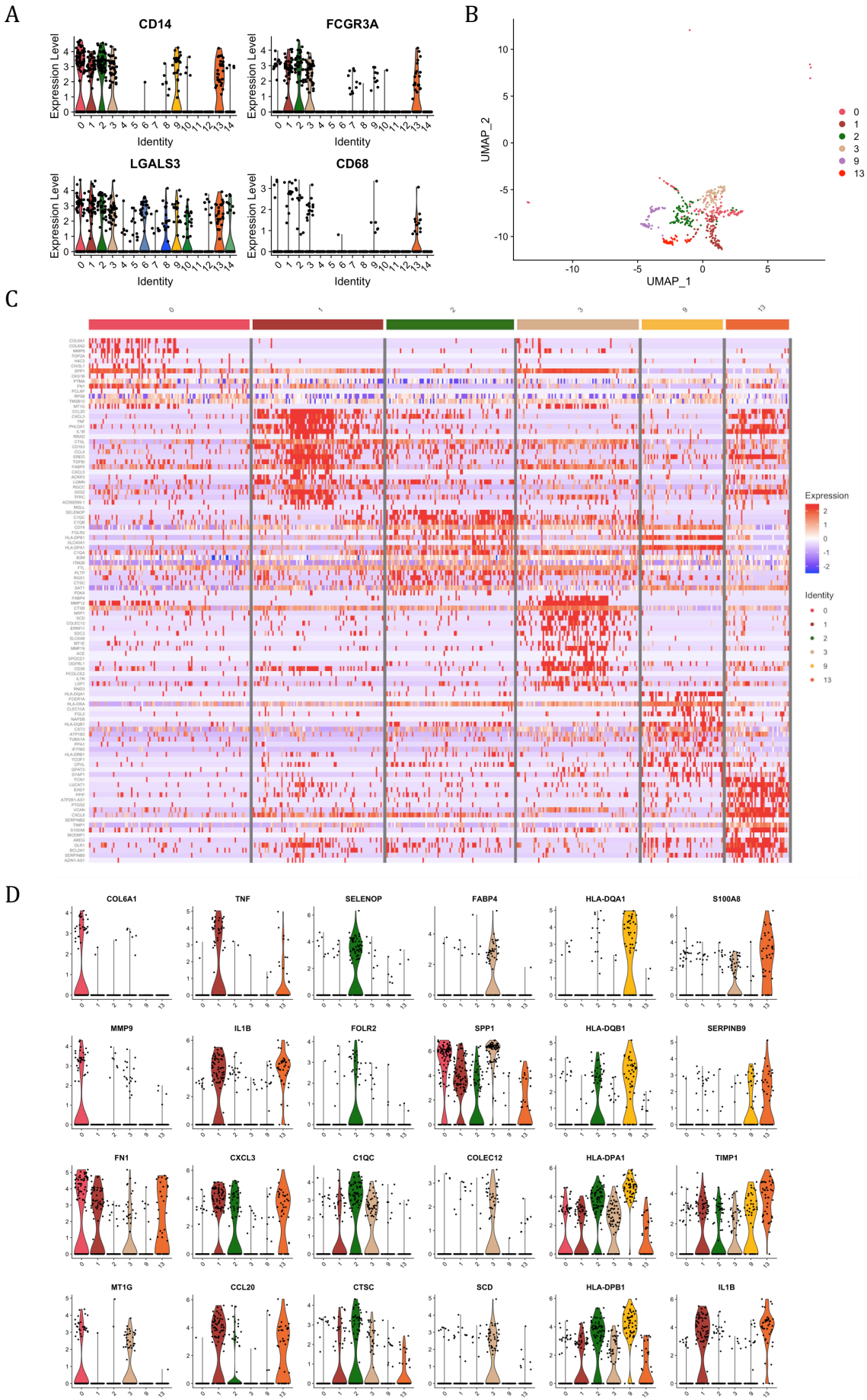
A
CD14
FCGR3A
LGALS3
CD68
Expression Level
Identity
B
UMAP_2
UMAP_1
0
1
2
3
9
13
C
Expression
Identity
D
COL6A1
TNF
SELENOP
FABP4
HLA-DQA1
S100A8
MMP9
IL1B
FOLR2
SPP1
HLA-DQB1
SERPINB9
FN1
CXCL3
C1QC
COLEC12
HLA-DPA1
TIMP1
MT1G
CCL20
CTSC
SCD
HLA-DPB1
IL1B

E

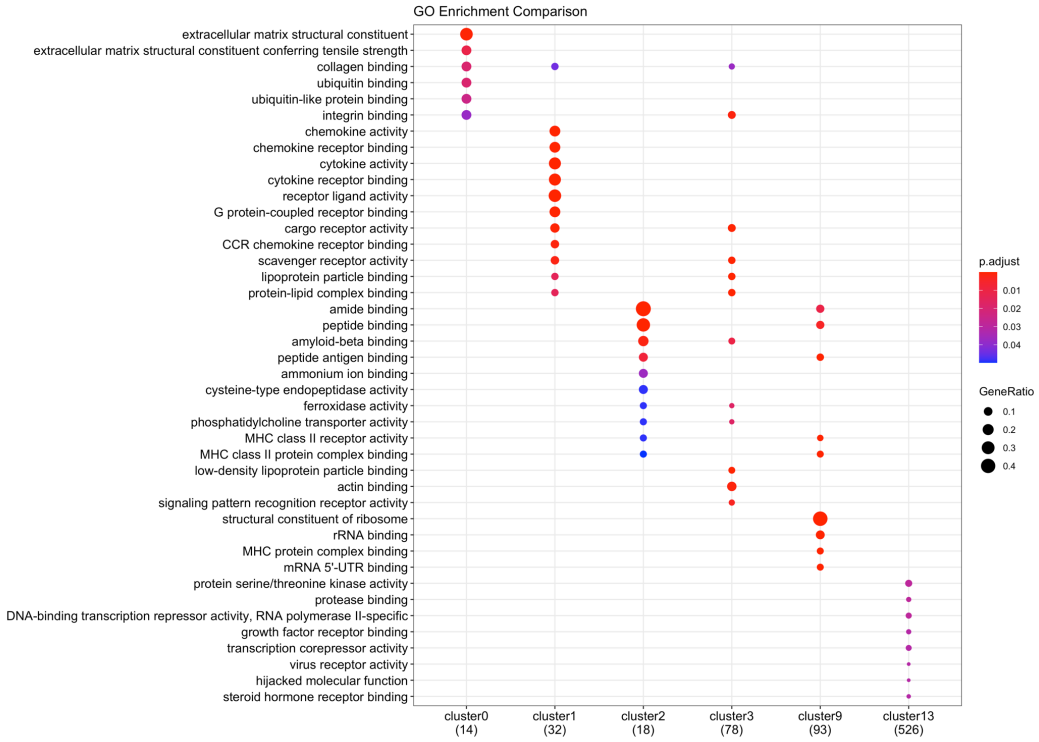
GO Enrichment Comparison
extracellular matrix structural constituent
extracellular matrix structural constituent conferring tensile strength
collagen binding
ubiquitin binding
ubiquitin-like protein binding
integrin binding
chemokine activity
chemokine receptor binding
cytokine activity
cytokine receptor binding
receptor ligand activity
G protein-coupled receptor binding
cargo receptor activity
CCR chemokine receptor binding
scavenger receptor activity
lipoprotein particle binding
protein-lipid complex binding
amide binding
peptide binding
amyloid-beta binding
peptide antigen binding
ammonium ion binding
cysteine-type endopeptidase activity
ferroxidase activity
phosphatidylcholine transporter activity
MHC class II receptor activity
MHC class II protein complex binding
low-density lipoprotein particle binding
actin binding
signaling pattern recognition receptor activity
structural constituent of ribosome
rRNA binding
MHC protein complex binding
mRNA 5'-UTR binding
protein serine/threonine kinase activity
protease binding
DNA-binding transcription repressor activity, RNA polymerase II-specific
growth factor receptor binding
transcription corepressor activity
virus receptor activity
hijacked molecular function
steroid hormone receptor binding
cluster0 (14)
cluster1 (32)
cluster2 (18)
cluster3 (78)
cluster9 (93)
cluster13 (526)
p.adjust
0.01
0.02
0.03
0.04
GeneRatio
0.1
0.2
0.3
0.4

F

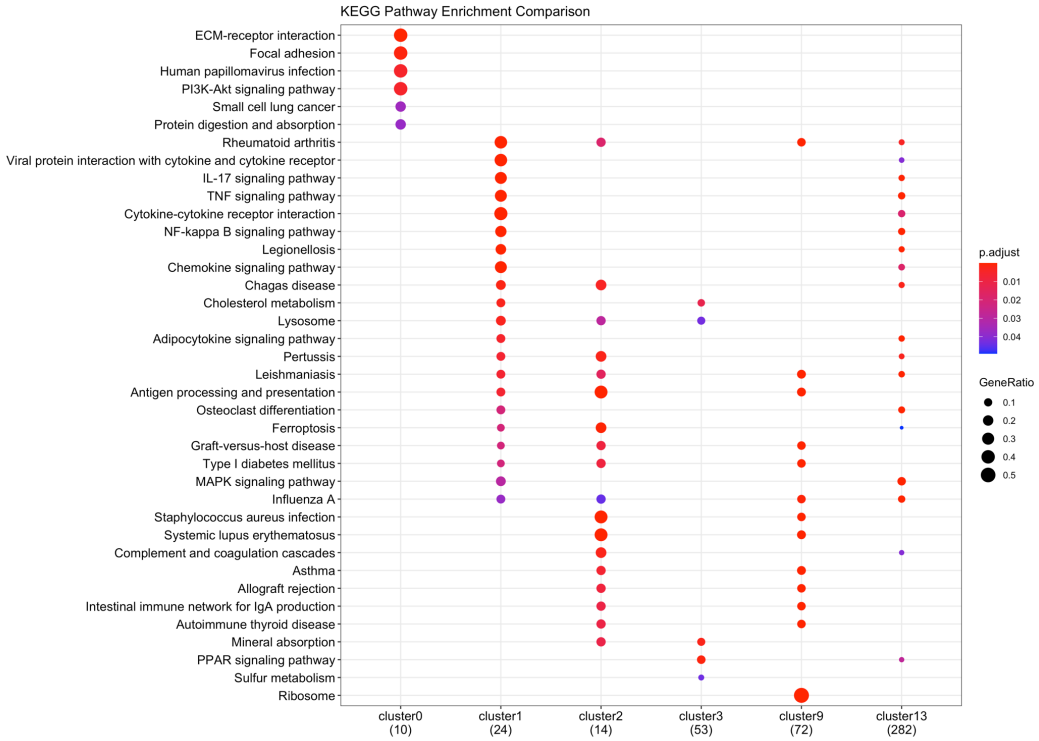
KEGG Pathway Enrichment Comparison
ECM-receptor interaction
Focal adhesion
Human papillomavirus infection
PI3K-Akt signaling pathway
Small cell lung cancer
Protein digestion and absorption
Rheumatoid arthritis
Viral protein interaction with cytokine and cytokine receptor
IL-17 signaling pathway
TNF signaling pathway
Cytokine-cytokine receptor interaction
NF-kappa B signaling pathway
Legionellosis
Chemokine signaling pathway
Chagas disease
Cholesterol metabolism
Lysosome
Adipocytokine signaling pathway
Pertussis
Leishmaniasis
Antigen processing and presentation
Osteoclast differentiation
Ferroptosis
Graft-versus-host disease
Type I diabetes mellitus
MAPK signaling pathway
Influenza A
Staphylococcus aureus infection
Systemic lupus erythematosus
Complement and coagulation cascades
Asthma
Allograft rejection
Intestinal immune network for IgA production
Autoimmune thyroid disease
Mineral absorption
PPAR signaling pathway
Sulfur metabolism
Ribosome
cluster0 (10)
cluster1 (24)
cluster2 (14)
cluster3 (53)
cluster9 (72)
cluster13 (282)
p.adjust
0.01
0.02
0.03
0.04
GeneRatio
0.1
0.2
0.3
0.4
0.5

G

H

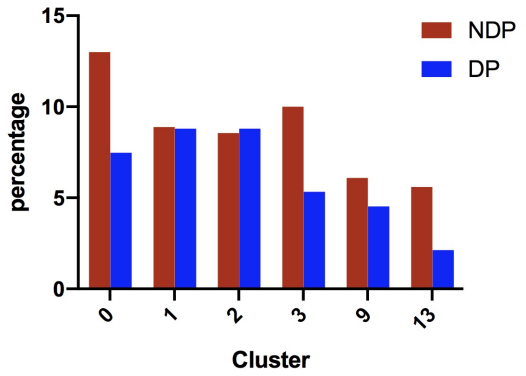

Figure 7. Characterization of Mono/Mφ in human AAA. A. Canonical markers, LGALS3, CD68, CD14, FCGR3A, highly expressed in cluster 0, 1, 2, 3, 9 and cluster 13; B. Clusters labelled Mono/Mφ were singled out in an individual UMAP; C. Top20 genes (weighted by avg_log FC, p_val_adj<0.05) of clusters 0, 1, 2, 3, 9, 13 were identified with FindAllmarkers in Seurat; D. Representative markers for each cluster(Cluster 0, 1, 2, 3, 9, 13);E. Gene Ontology (GO) for all the six clusters in Mono/Mφ; F-G. Pathway analysis of Mono/Mφ. KEGG Pathway Enrichment Comparison (F) and Reactome Pathway Enrichment Comparison (G) among the six clusters of Mono/Mφ; H. Percentage of each cluster from Mono/Mφ cells in each sample. Notes: NDP, non-dilated part of AAA; DP, dilated part of AAA.

4.4 Heterogeneity of VSMC and Adventitial Fibroblasts in Human AAA

Phenotypic switch of VSMC has received increasing attention in the study of AAA pathophysiology (Wu et al., 2020). Interestingly, recent single-cell studies have demonstrated a close relationship between VSMC and fibroblasts and the existence of "fibromyocytes" (or "modulated SMC") (Wirka et al., 2019; Pedroza et al., 2020). The characteristics of VSMC and fibroblasts were thus described together in this section.

As depicted in ***Figure 5D***, cluster 6, 8, and 12 corresponded to "VSMC and fibroblasts", which characterized by the expression of markers like ACTA2, TAGLN, PI16, FBLN1, DCN and C11orf96 (***Figure 8A*****)**. The top 10 markers of cluster 6, 8, and 12 can be found in ***Table S2***. Since previous studies reported a previously underestimated complexity of VSMC and fibroblasts transcriptional landscape (Wirka et al., 2019; Pedroza et al., 2020), unsupervised clustering from cluster 6, 8 and 12 was performed and seven distinct subpopulations popped up, as depicted in ***Figure 8B-C***. Top DEGs (avg_logFC>0 & p_val_adj <0.05) of each subcluster were then compared with the remaining 6 subclusters, as shown in ***Figure 8D***. Basing on these markers, subclusters VF3, VF5, and VF7 were labeled as VSMC, while VF 1, VF2, and VF4 were considered as fibroblasts.

Interestingly, a previously reported gene expression signature identifying 'modulated' VSMC (FN1, TNFRSF11B, COL1A1, LUM, SERPINE1, LGALS3)(Wirka et al., 2019; Pedroza et al., 2020), was also detected in this dataset, with higher expression in VF3 compared to VF5 and VF7 (***Figure 8E)***. Moreover, other genes like TIMP1, DCN and POSTN were upregulated in VF3 compared to VF7 (***Figure 8F*** and ***8H***). DEGs in non-dilated *vs* dilated samples relative to cluster VF3 are shown in ***Figure 8G***. Furthermore, VF3 cell cluster also expressed genes like VCAM1, one of the markers defining the "VSMC intermediate cell state" (SEM cells) (Pan et al., 2020), as well as COL1A1 and COL3A1, characterizing fibrochondrocytes. VCAM1 positive cells in VF3 accounted for 28.1%, while they were not detected in VF5 and VF7 clusters (***Figure 8I***). Of notice, loss of markers

of MSC NT5E and ENG, expected in VSMC-derived SEM cells (Pan et al., 2020), was not observed in VF3 (***Figure 8I***).

Subpopulation VF7 included 'contractile' VSMC, expressing MYH11 (Leeper and Maegdefessel, 2018), COL4A1, COL18A1. Interestingly, one of the top markers in VF7, MALAT1, was reported to be part of a ternary complex that can repress expression of genes coding for contractile protein in thoracic aortic aneurysm progression (Wu et al., 2020). Expression of TIMP1, a classical metalloproteinase inhibitor, involved in remodeling of the extracellular matrix (Busch et al., 2016), was remarkably high in cluster V5. However, these populations accounted for about 0-5% in each group (***Figure 8J***), deviating from what expected in vascular wall.

Adventitial fibroblasts (AFs) play a crucial role in vascular remodeling (Tinajero and Gotlieb, 2020). As the most enriched cell type in the adventitia, AFs present numerous subtypes with different behavior and morphology (Coen et al., 2011). In line with this observations, different AFs subpopulations (VF1, VF2, and VF4 clusters) were identified in this study (***Figure 8C-E***). Currently, no markers are available to specifically identify AF; however, expression of THY1, PI16, COL14A1, MMP3, CXCL14 (LeBleu and Neilson, 2020) and SFRP2 (Tabib et al., 2018) (***Figure 8K***), which participate in matrix production and inflammatory process, strongly suggests AFs identity.

The last interesting subset in this cohort, VF6, was considered as "neuron-like", basing on the expression genes like SCN7A (García-Villegas et al., 2009), HBEGF (Kushwaha et al., 2019), HMOX1 (Nitti et al., 2018), CRLF1 (Looyenga et al., 2013), GPC3 (Oikari et al., 2016), NR2F1(Zhang et al., 2020) (***Figure 8E, Figure 8L***). Importantly, these cells were exclusively present in the sample of "Non-dilated_Self group", as shown in ***Figure 5C*** *and* ***Figure8B-C***.

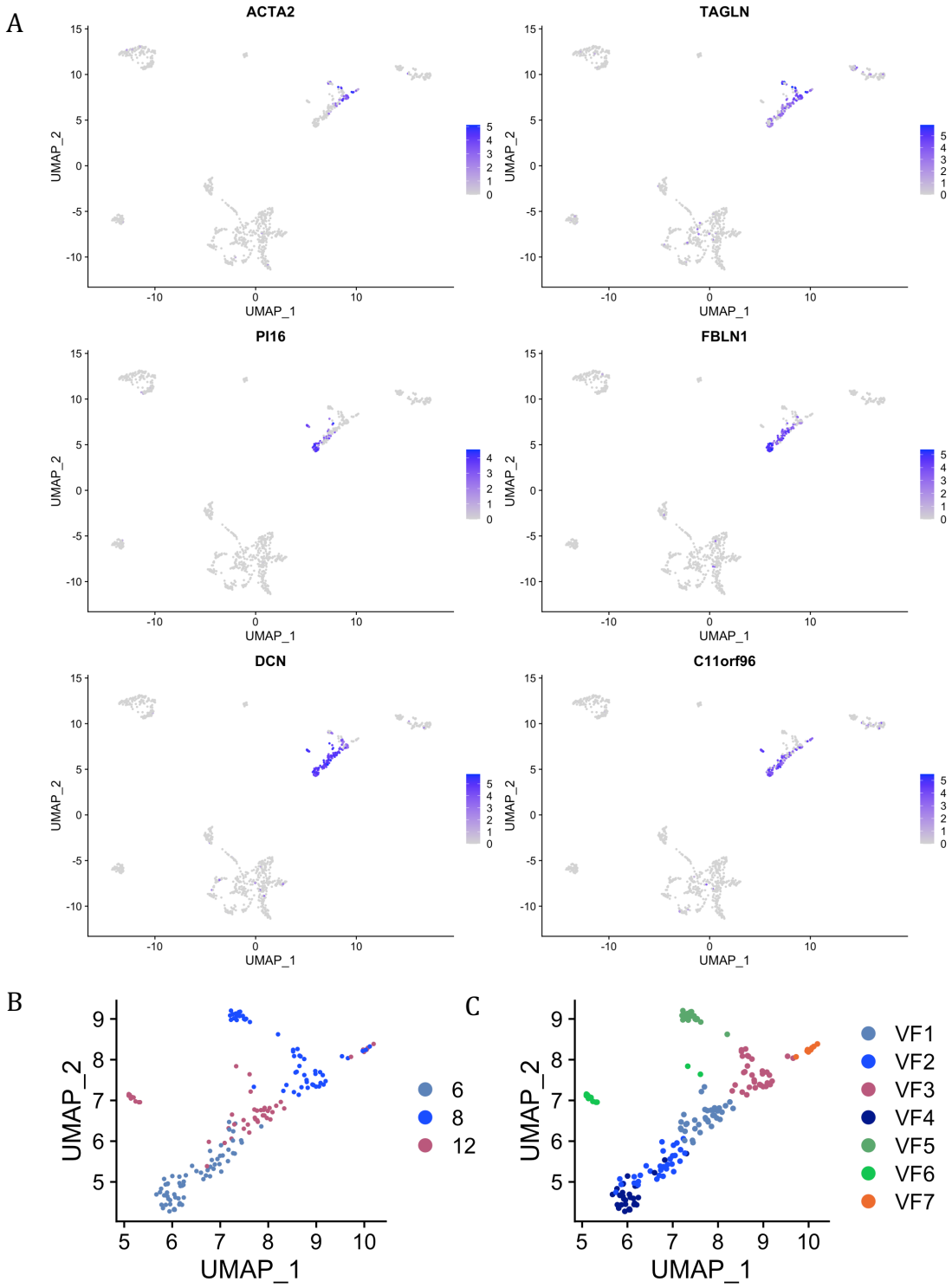
A
ACTA2
TAGLN
PI16
FBLN1
DCN
C11orf96
UMAP_1
UMAP_2
B
6
8
12
C
VF1
VF2
VF3
VF4
VF5
VF6
VF7

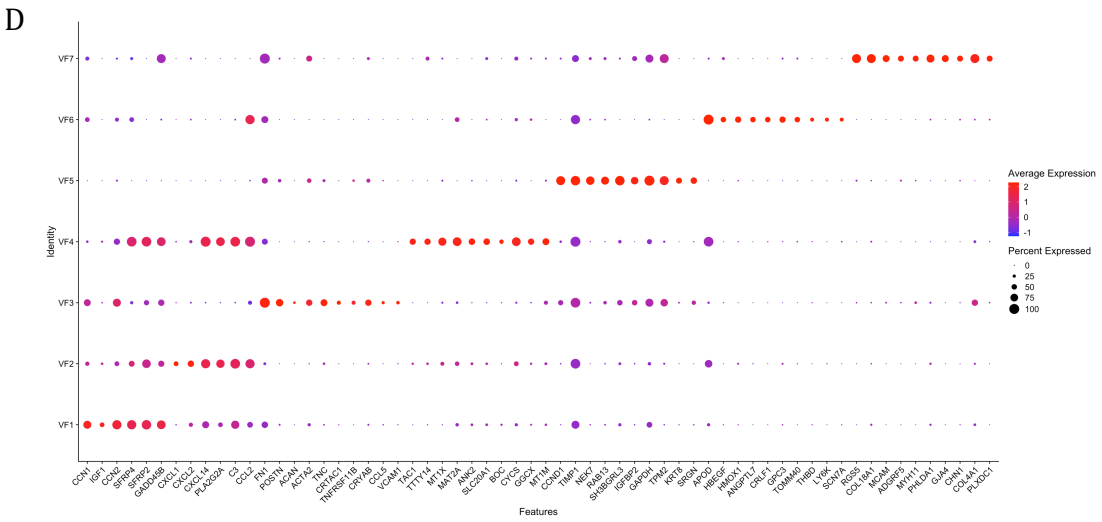
D
VF7
VF6
VF5
VF4
VF3
VF2
VF1
Identity
Features
Average Expression
Percent Expressed

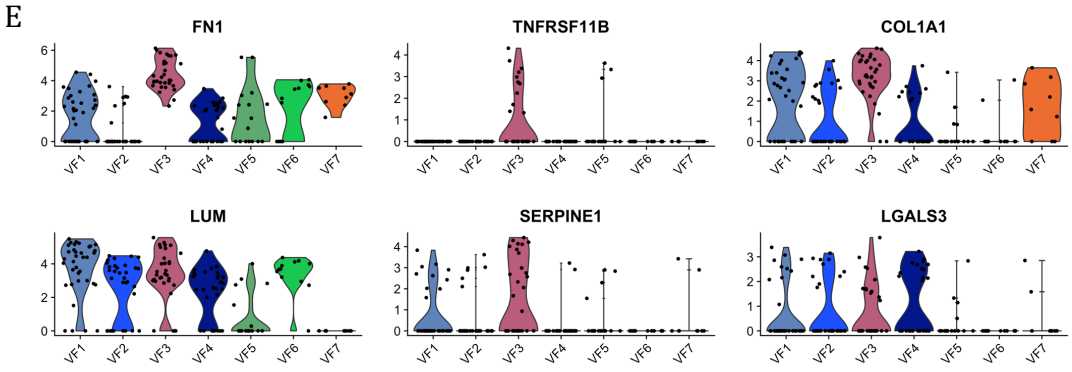
E
FN1
TNFRSF11B
COL1A1
LUM
SERPINE1
LGALS3

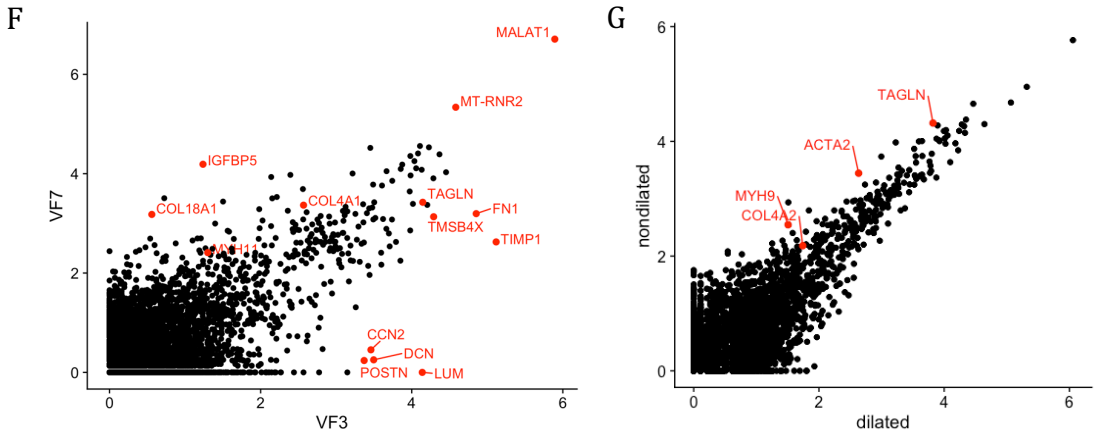
F
MALAT1
MT-RNR2
IGFBP5
COL18A1
COL4A1
TAGLN
FN1
TMSB4X
TIMP1
MYH11
CCN2
DCN
POSTN
LUM
VF7
VF3

G
TAGLN
ACTA2
MYH9
COL4A2
nondilated
dilated

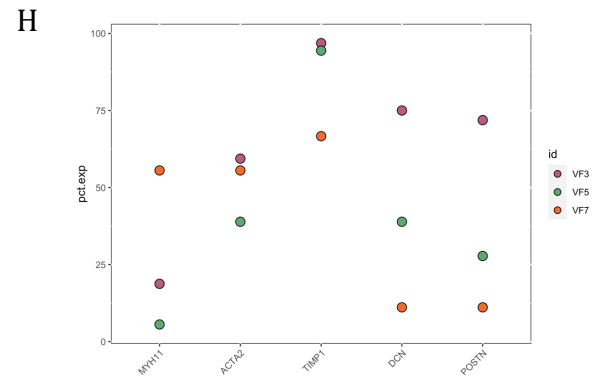
H
pct.exp
MYH11
ACTA2
TIMP1
DCN
POSTN
id
VF3
VF5
VF7

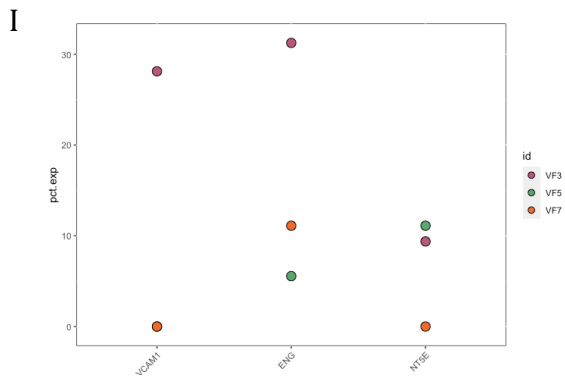
I
pct.exp
VCAM1
ENG
NT5E
id
VF3
VF5
VF7

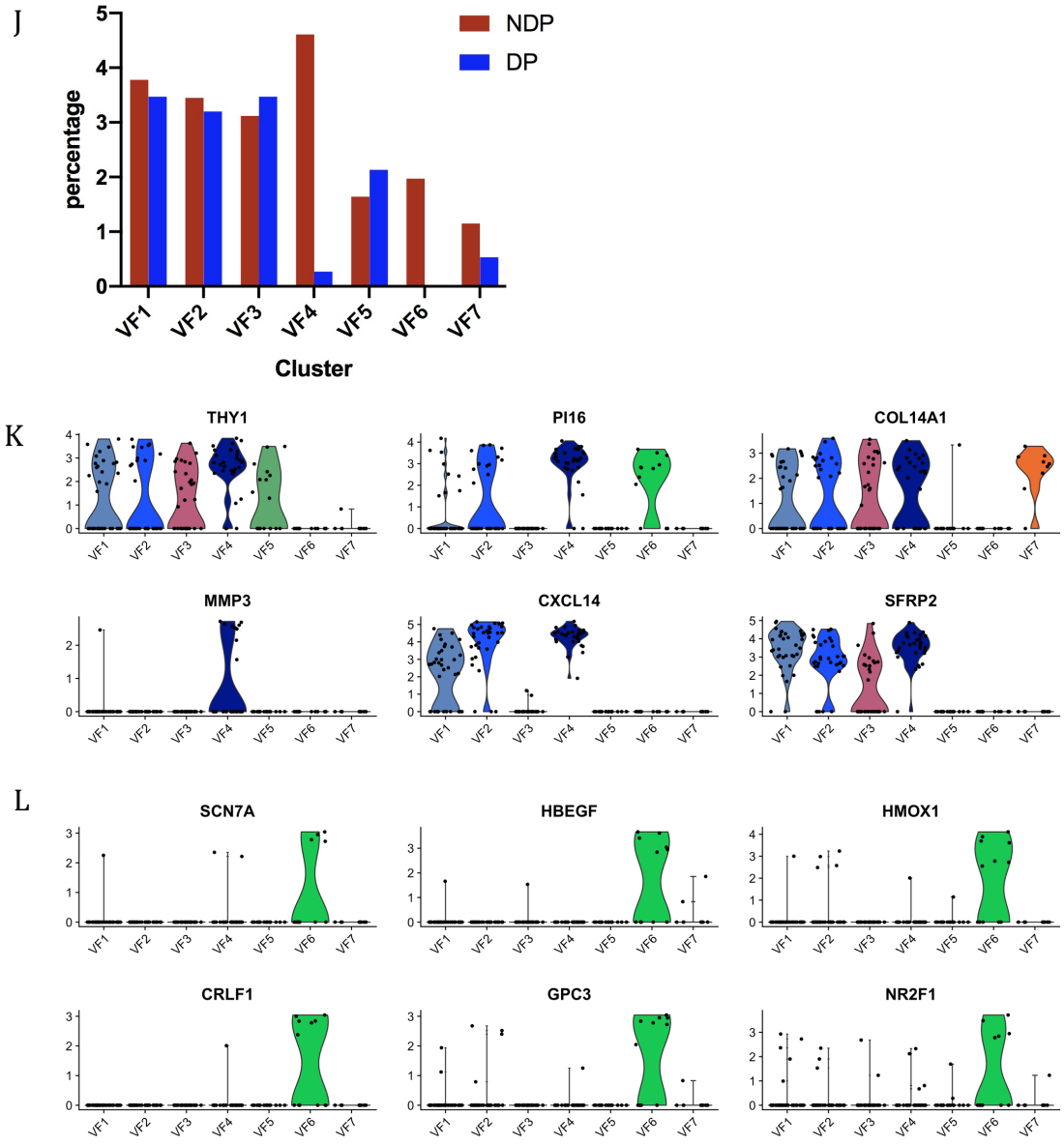

Figure 8. Characterization of VSMC and fibroblasts in human AAA. A. Classical markers confirmed in Cluster 6, 8, and 12; B-C. UMAP revealed the heterogeneity among Cluster 6, 8 and 12 (B). Unsupervised specific clustering on these three clusters identified 7 subclusters (C) with different functions; D. Top differentially expressed genes among the 7 subclusters; E. Markers defining 'modulated' VSMC (Wirka et al., 2019; Pedroza et al., 2020); F. Scatter plot shows the average expression of genes characterizing subcluster VF3 and VF7; G. ACTA2, TAGLN, COL4A2, MYH9 decreased from NDP to DP; H-I. dot plot revealed the cell percentage among clusters; J. altered percentage of each subcluster in NDP vs DP; K-L. Violin plot representing markers in adventitial fibroblasts (K, subcluster 1, 2, 4) and in neurons (L, subcluster 6). Notes: Pct.exp, percentage of positive cells in each cluster; feature.plot, genes to plot.VF3, 5 and 7, three subpopulations of vascular smooth muscle cell. NDP,non-dilated part. DP, dilated part.

4.5 Two Distinct Gene Expression Profiles in ECs

Two clusters (cluster 10 and 14) were identified as ECs (***Figure 5D***), characterized by high expression levels of VWF and PECAM1 (***Figure 9A*)**. Interestingly, canonical ECs marker CDH5, previously identified to be equally expressed by all ECs clusters in a mouse study (Kalluri et al., 2019), was predominantly expressed in cluster 10 (***Figure 9A***). Other canonical EC-specific markers, like FLT1 and angiogenesis-related SDPR, PTPRB and ECSCR, followed the same pattern (***Figure 9A***).

Distinct gene expression patterns between cluster 10 and 14 were thus explored and top markers for each cluster plotted in ***Figure 9B*.** Cluster 10 was mostly characterized by the expression of genes related to lipid transport (FABP4), inflammatory state (ETS2 (Cheng et al., 2011)) and angiogenesis or vasculogenesis (MMRN2 (Pellicani et al., 2020), AKAP12 (Benz et al., 2020), IGFBP3 (Dallinga et al., 2020), ADAMTS1 (Lambert et al., 2020), ACKR3 (Wei et al., 2020)). Top markers in cluster 14 were instead involved in regulation of coagulation (GIMAP4, GIMAP7 (Sabater-Lleal et al., 2019), RHOB (Pronk et al., 2019)), cholesterol binding (TSPO(Biswas et al., 2018)) and metabolism (TXNIP (Domingues et al., 2020)). Functional role of other top markers in cluster 14, like GLT8D1, LRRC28, STX8 and FKBP4, remains so far undefined.

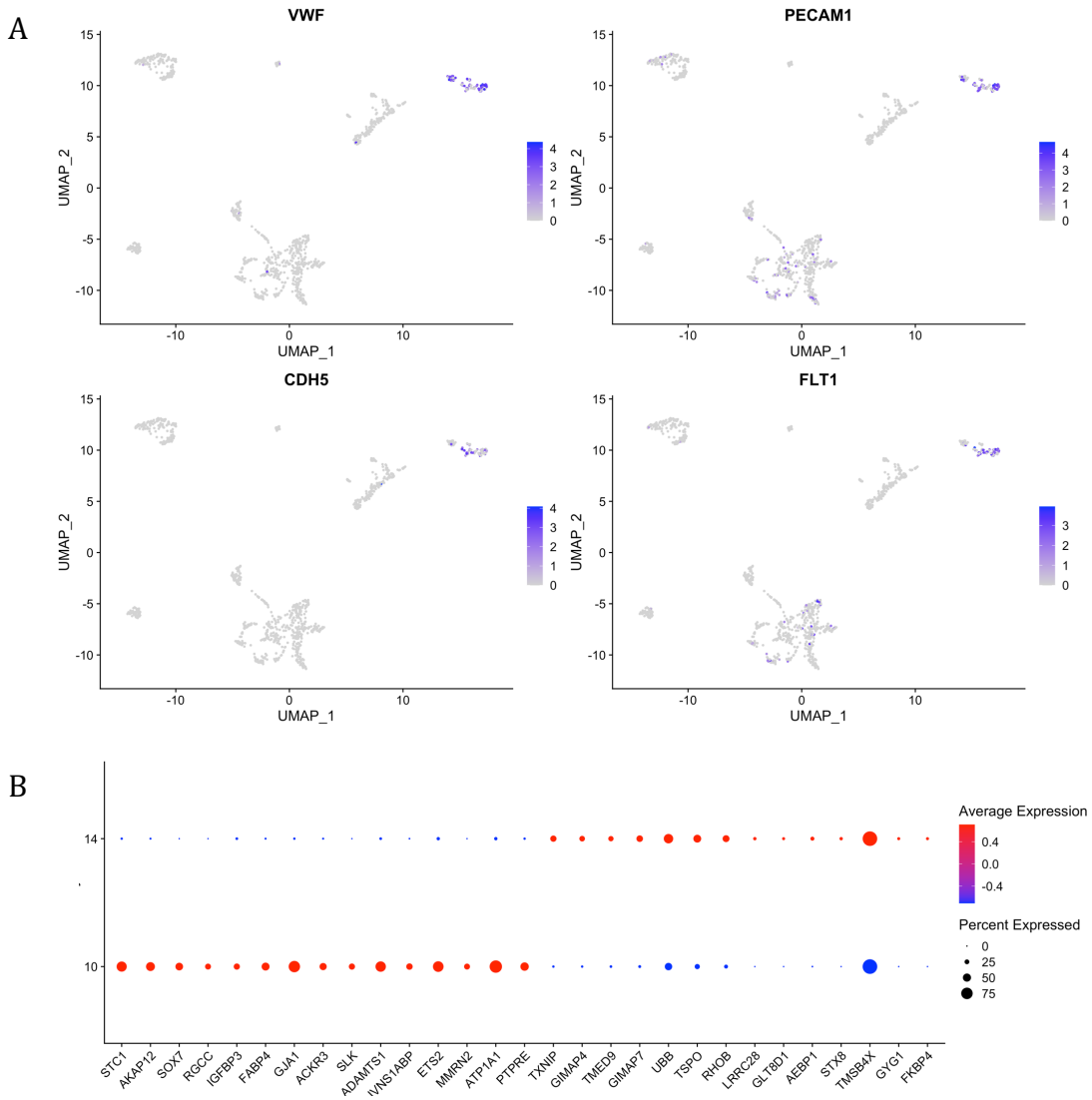

Figure 9. Characterization of two distinct ECs clusters. A. Featureplots point out highly expressed VWF and PECAM1 in cluster 10 and 14, indicating that both are ECs; B. Top markers relative to cluster 10 and 14, identified with FindAllmarkers in Seurat package.

4.6 T cell and B cell Increased from the Non-dilated Part to the Dilated Part

T cells (TC) were detected in cluster 4 and 7, as shown in ***Figure 5E*** *and* ***Figure 10A***. In particular, cluster 4 and 7 were respectively identified as $CD4^+$ TC (CD4, CCR7, ***Figure 10A***) and $CD8^+$TC (CD8, GZMA, ***Figure 10A*****)**. Overall, TC percentage increased from non-dilated (10.69%) to dilated AAA tract (18.4%) (both $CD4^+$ TC and $CD8^+$ TC, from 6.58% to 10.67% and from 4.11% to 7.73%, ***Figure 10B***.

CD79A and MS4A1-highly expressing B cells (BC) were identified in cluster 11, as shown in ***Figure 10C***. Furthermore, plasma cells were detected in cluster 5 ***(Figure 10D)***. Both TC and BC occupied more proportions in the dilated part than those in the non-dilated part ***(Figure 10B)***, indicating their contributor roles in the process of AAA formation.

A

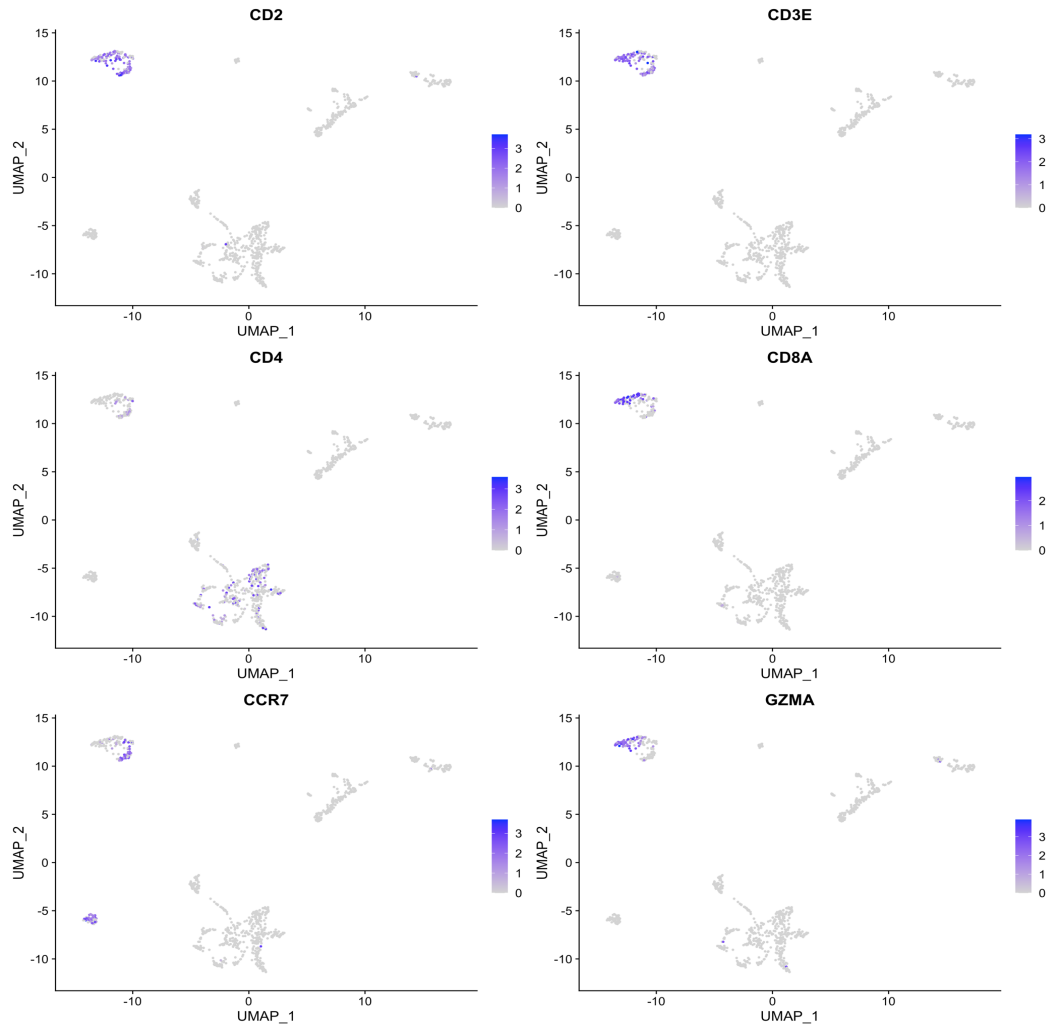

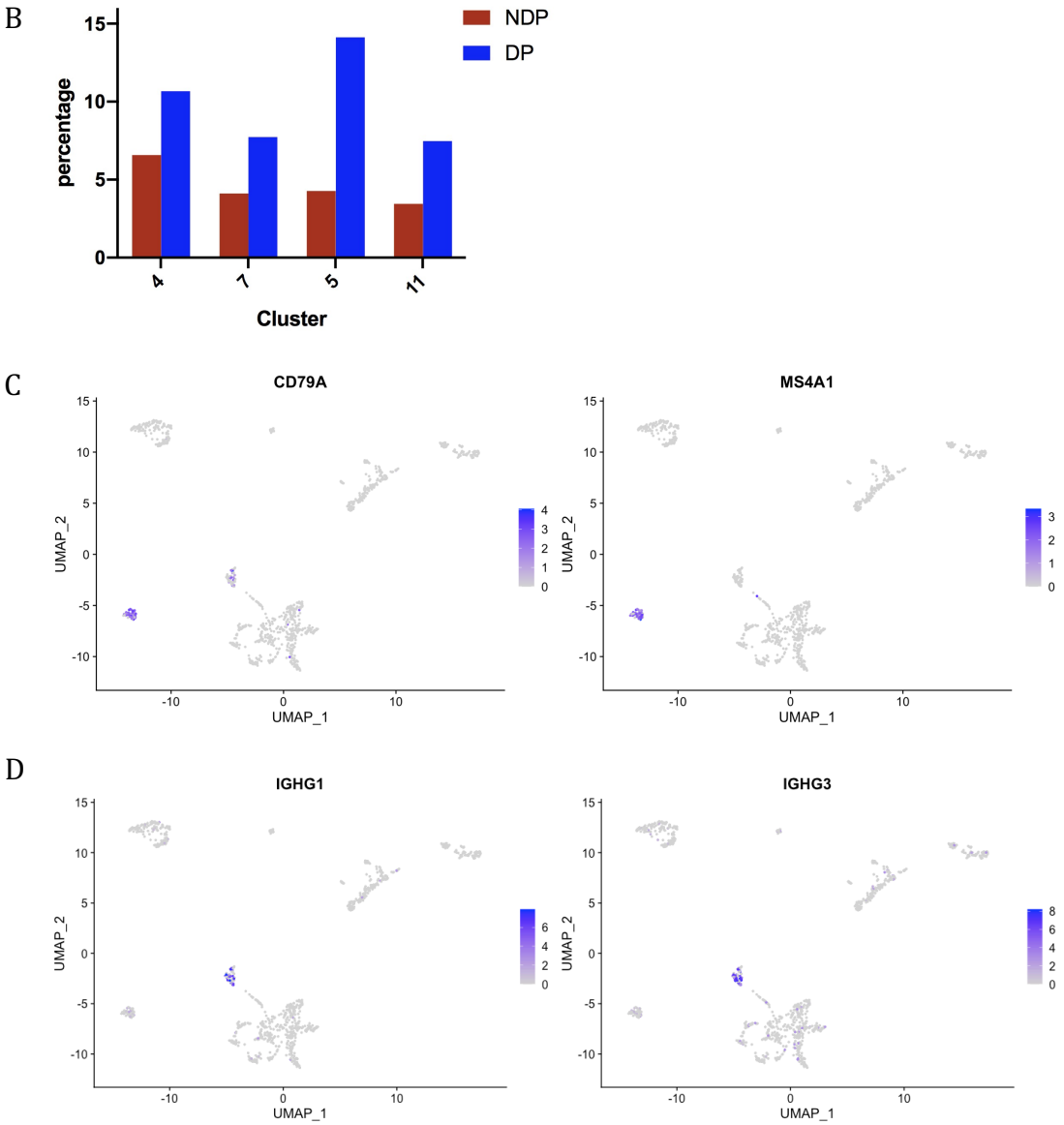

Figure 10. Markers of T cell and B cell. A. Featureplots for markers of TC (CD2, CD3E), CD4⁺ TC (CD4, CCR7) and CD8⁺ TC (CD8A, GZMA); B. Altered proportions of TC, BC and plasma cells. Cluster 4 (CD4⁺ T cells), cluster 7 (CD8⁺ T cells) cluster 5 (plasma cells) and cluster 11 (BC); C. Featureplots for markers of BC in cluster 11 (CD79A and MS4A1); D. Markers of plasma BC. Notes: TC,T cells; BC, B cells.

5. DISCUSSION

5.1 The Study-Control Group Setting in the AAA

Although AAA is one of the most life-threatening cardiovascular diseases, mechanistic insights on its development and progression are still lacking and, as a consequence of this, targeted pharmacological treatment is still unavailable. To delineate the mechanism underlying AAA pathophysiology, both animal models and *ex vivo/in vitro* human samples have been utilized. Regarding animal models, the selection of a control group for AAA studies usually directs to strains like C57BL/6J mice or Yucatan mini-pigs (Maegdefessel et al., 2014; Li et al., 2018). In human studies, the control samples are mostly collected either from OSR for ruptured AAA (Gäbel et al., 2017) or from organ donors (Biros et al., 2014). From this point of view, the study-control group setting (AAA specimens *versus* the healthy aortic fragments or elective AAA *versus* rupture AAA) prevents from exploring the molecular differences within different sites of the individuals with AAA, especially the more upstream non-dilated aneurysm neck and the downstream dilated part of AAA. The non-dilated aortic neck of AAA may serve as an internal control. Thus, another pattern of study-control group setting can refer to the two parts of AAA, similar to a previous PVAT transcriptomic study where the researchers compared gene expression patterns of adipose tissue around the dilated AAA with that of the non-dilated aortic neck(Piacentini et al., 2019).

In this study, gene expression patterns of non-dilated aortic neck with the most dilated portion at the very site of AAA were compared (***Figure 1)***. Such a strategy allows to set an internal control from the same individual, thus disregarding the genetic background "noise" arising from inter-individual variability. However, the anatomical structures of the aneurysmal aorta can sometimes pose technical challenges to surgeons, making it difficult to excide the non-dilated fragment. Furthermore, other situations in which the internal control samples may not be considered as the ideal ones are when the maximum diameter is too large (like 11cm) or if it is believed to be an infectious AAA.

5.2 Digestion Protocol Matters in the scRNA-seq Study

An optimal digestion protocol enables reliable data. It requires neither over-digestion nor under-digestion (Chavkin and Hirschi, 2020), but the best combination of different enzymes, concentrations, and digestion times. A recent publication about VSMC in aortic aneurysm of Marfan's syndrome (Pedroza et al., 2020) set Liberase TM and elastase as the main component of the digestion solution. Another study adopted collagenase, hyaluronidase, and DNase as cocktails in the enzymatic digestion for mouse normal aorta (Kalluri et al., 2019).

In this study, we applied two digestion protocols as described in the methods, resulting in similar cell clusters. Unexpectedly, VSMCs, one of the main components in the vascular wall, turned out way fewer than predicted. A possible reason may be the suboptimal digestion protocol. One neglected source is the lengthy manual processing time of mincing samples for digestion(Williams et al., 2020a). Another potential reason is the 40-μm strainer we used during the preparation stage which may not be wide enough for the VSMCs to pass through and may preclude them for following 'water-in-oil' steps.

5.3 Two Ways to Annotate the Cell Clusters

Clusters to labeling with cell type identities is one of the most critical steps in the analysis of scRNA-seq data. Currently, manual and automatic labeling are the two major ways to annotate the clusters with cell type identities. Manual annotation requires abundant knowledge about the cell types of interest and substantial time. Hence, to facilitate this step, the automatic annotation is then introduced to determine potential cellular identities. However, it has to be addressed that efficiency of automatic annotation is strongly affected by the reference databases. These automatic methods mainly include scMap (Kiselev et al., 2018), SingleR (Aran et al., 2019), Garnett (Pliner et al., 2019), CellAssign (Zhang et al., 2019a), CHETAH (de Kanter et al., 2019) and scCATH (Shao et al., 2020).

In this study, cell clusters or cell subpopulations were labeled by manual annotation, as the automatic method resulted in either too many subpopulations

or some subpopulations presenting without specific biological insights (results not shown in this thesis).

5.4. Innate Immune and Adaptive immune May Differ in the Non-dilated Part and the Dilated Part of the AAA

Based on the human and animal research studies, current theories on the pathogenesis of AAA are mainly composed of four aspects: (1) Immune-driven; (2) Consequence of atherosclerosis and thrombosis; (3) Inherited and (4) biomechanical factors (Golledge, 2019). In this context, this study provides a 'snapshot' of cell populations characterizing human AAA at single cell level, thus contributing to further global mechanistic hints on AAA formation.

Among immune cells, Mφ were the largest population in both, the non-dilated part as well as the dilated part. These are involved in inflammatory responses (IL-17, TNF, NFκB signaling pathway, etc.), antigen presentation and cholesterol metabolism, etc., which were in agreement with previous studies (Williams et al., 2018). One of these phenotypes, resident Mφ, expressing markers like SELENOP, FOLR (Willemsen and de Winther, 2020) was also detected in this study, accounting for around 9% of the total cells. For a long time, local proliferation has represented the main model of Mφ accumulation in the process of atherosclerosis (Robbins et al., 2013). However, a recent lineage study revealed that resident Mφ in the intima partly originated from recruited monocytes during the early process (Williams et al., 2020b). However, whether this phenomenon also occurs in the early stage of AAA requires further experiments. Furthermore, loss of spatial information leaves a question mark on the precise localization of these cell population in the aortic wall. This population also shared the function of 'antigen processing and presentation' with DCs, which was one of the confirmed characteristics among resident Mφ (Williams et al., 2020b).

In contrast to the scRNA-seq study of murine AAA models (Zhao et al., 2020), we detected a cluster corresponding to 'fibroblast-like Mφ' in this cohort. These cells are mainly related to the extracellular matrix organization or degradation

(markers: MMP9, COL6A1). The origin of such cluster (fibroblast-derived? VSMC-derived? Mφ-derived? or other cell types?) remains to be elucidated.

The significant percentage reduction of Mφ in dilated AAA compared to the non-dilated internal control represents another intriguing difference with the murine AAA study (Zhao et al., 2020) where the Mφ increased in AAA. This difference can be due to the different nature of controls. So far, to the best of my knowledge, no studies have yet compared these two parts from one individual's AAA at the single cell level. A similar approach was employed in the transcriptomic study of PVAT (Piacentini et al., 2019), supporting the reliability of the results.

Another debated issue is the role of MMPs in AAA, that if the MMPs serve as a cause or are an effect. MMPs (like MMP3) were downregulated in dilated AAA in this study. While MMPs were previously demonstrated to be upregulated in diseased ones (Maegdefessel et al., 2013; Maguire et al., 2019). Further investigations are needed to unveil the reasons underlying these opposing results.

T cells, B cells, and plasma cell percentages were found to be augmented in dilated AAA, indicating a possible role in AAA formation.

Based on these observations, we hypothesize that the non-dilated neck of AAA may represent the early stage of AAA disease, while the dilated part may reflect the late stages, ultimately ending in rupture. Macrophages and monocytes may be more active in non-dilated part, while T cells, B cells, and plasma cells may undergo strong activation in the dilated part. This hypothesis requires more robust experimental validation and support of scRNA-seq data from other labs.

5.5 Structural Cells Involve in AAA Development

VSMCs and fibroblasts, as structural cells in charge of maintenance of vascular structure and integrity, can contribute to vascular remodeling (Kuwabara and Tallquist, 2017; Wu et al., 2020). In particular, VSMC may undergo 'phenotype switching' through the course of aortic aneurysm and atherosclerosis (Wu et al., 2020). During this process, TGFβ signaling was demonstrated to play a key role, as reported by a recent murine Marfan Syndrome study (Pedroza et al., 2020).

Our dataset showed that only a minor percentage of sequenced cells were actually VSMCs (5.5%, 54/983) which were further identified as three subpopulations (VF3, VF5, and VF7). VF7 showed high expressions of canonical markers of contractile VSMC like MYH11, etc., while VF3 was the newly named 'modulated VSMC' or 'fibromyocytes' (Wirka et al., 2019; Pedroza et al., 2020) for their defining markers (like FN1, TNFRSF11B, SERPINE1, and LGALS3). In particular, canonical markers (ACTA2, TAGLN) characterizing VF7 were less expressed in VF3. Furthermore, we observed a gradient towards down-regulation of contractile genes expressed by VF3 cluster from the non-dilated to the dilated AAA fragment, which may support a loss of contractility of VSMC residing at the dilated site of AAA. Another interesting observation in subpopulation VF3 was that, the 'modulated VSMC' contained both the cell types of intermediate cell state of VSMCs and fibrochondrocytes, which was in alignment with a recent study (Pan et al., 2020). Importantly, markers that defined the intermediate cell state of VSMCs (VCAM1(Pan et al., 2020)) were not expressed in VF5 and VF7, further corroborating the peculiarity of this cluster. The intermediate cell state of VSMCs were also described in a cardiac outflow tract study (Liu et al., 2019). Increasing sample size and integrating human results with data from AAA animal models represent crucial point in collecting further information on the contribution of VSMC phenotype to AAA progression.

A major concept in the 'inside-to-outside' theory model, is that vascular inflammation initiates in ECs in the intimal layer, to ultimately spread to the adventitia (Lin et al., 2019). This was also observed from the top-expressed markers in the ECs as shown in this study. On the other hand, the 'outside-to-inside' theory model claims that inflammation starts from the PVAT to the intima. During this process, inflammatory cytokines IL-18 is induced by the leptin and FABP4 from the PVAT, contributing to AAA formation (Liu et al., 2020). A recent scRNA-seq study has revealed the role of PVAT-derived mesenchymal stem cells in vascular regeneration(Gu et al., 2019), though, it would also be interesting to

test this hypothesis in AAA development by profiling PVAT transcriptional landscape at single cell level.

In either 'inside-to-outside' theory or 'outside-to-inside' model, our dataset showed that adventitial fibroblasts suffered a significant loss along with AAA progression. Similarly to other single-cell studies (Wirka et al., 2019; Pedroza et al., 2020; Tillie et al., 2020), heterogeneities of fibroblasts were also observed here, one of which may also serve as contributors to immune responses (Krausgruber et al., 2020).

5.6 Limitations in this Study and in General scRNA-seq Studies

The main limitation of this study is represented by the reduced number of sequenced cells available for downstream analysis, leading to a potential bias on cluster annotation and, thus interpretation of results. However, the study presented in this thesis represents only the starting point towards creation of a more comprehensive scRNA-seq dataset on huan AAA. In the future, more samples and more cells will be included, thus allowing deeper investigation of rare cell types. Another drawback is that the results here are based on computational analysis and literature search, lacking experimental validation with a more functional perspective (cluster localization, functions or mechanistic insights on AAA). As previously discussed, dissociation protocols could significantly affect the throughput(quality/number/type) of sequenced cells, especially for VSMCs which resulted to be way fewer than expected in this study.

From a broader perspective, previous reviews have listed several limitations of scRNA-seq studies(Williams et al., 2020a; Zernecke et al., 2020). Technically, transcripts cannot be entirely covered because the results represent a 'snapshot' during sampling (Zernecke et al., 2020). Moreover, the reads obtained from scRNA-seq are much fewer than the ones from bulk-sequencing. Another limitation is the loss of spatial information in scRNA-seq analysis, leaving the question of cluster localization yet open.

6. SUMMARY AND PERSPECTIVES

In summary, this study provided direct insights into human AAA cell composition at the single cell level. In particular, the analysis of scRNA-seq dissected the cellular heterogeneities among various cell types characterizing human AAA. A bioinformatic pipeline has been established for cluster identification and labelling. This study firstly described and compared the different expression profiles/cell clusters in the non-dilated aortic neck versus the dilated part of AAA, thus providing novel insights in AAA development and progression.

ScRNA-seq is a robust tool to measure changes in gene expression, even if the gene's spatial context drops out during cell separation. Spatial solved transcriptomics is thus a complementary method to fill this gap. Two complementary spatial solved transcriptomics methods, the seqFISH+ (Eng et al., 2019) and the Slide-seq (Rodriques et al., 2019), have paved the way closer to the spatial transcriptome-wide data at single cell level (Burgess, 2019). Besides, the commercialization of spatial transcriptomics (Ståhl et al., 2016) by 10X Genomics Chromium company, also called *VISIUM*, provides possibilities to obtain both transcriptomic and spatial information at the same time. Furthermore, many other state-of-art methods like multi-omics (Krausgruber et al., 2020), CyTOF (Fernandez et al., 2019) can also be utilized to dissect the insights of AAA.

7. REFERENCES

Ailawadi, G., Moehle, C.W., Pei, H., Walton, S.P., Yang, Z., Kron, I.L., Lau, C.L. and Owens, G.K., 2009. Smooth muscle phenotypic modulation is an early event in aortic aneurysms. J Thorac Cardiovasc Surg 138, 1392-1399.

Aran, D., Looney, A.P., Liu, L., Wu, E., Fong, V., Hsu, A., Chak, S., Naikawadi, R.P., Wolters, P.J., Abate, A.R., Butte, A.J. and Bhattacharya, M., 2019. Reference-based analysis of lung single-cell sequencing reveals a transitional profibrotic macrophage. Nat Immunol 20, 163-172.

Azizi, E., Carr, A.J., Plitas, G., Cornish, A.E., Konopacki, C., Prabhakaran, S., Nainys, J., Wu, K., Kiseliovas, V., Setty, M., Choi, K., Fromme, R.M., Dao, P., McKenney, P.T., Wasti, R.C., Kadaveru, K., Mazutis, L., Rudensky, A.Y. and Pe'er, D., 2018. Single-Cell Map of Diverse Immune Phenotypes in the Breast Tumor Microenvironment. Cell 174, 1293-1308.e36.

Badger, S.A., Jones, C., McClements, J., Lau, L.L., Young, I.S. and Patterson, C.C., 2011. Surveillance strategies according to the rate of growth of small abdominal aortic aneurysms. Vasc Med 16, 415-421.

Bagnoli, J.W., Ziegenhain, C., Janjic, A., Wange, L.E., Vieth, B., Parekh, S., Geuder, J., Hellmann, I. and Enard, W., 2018. Sensitive and powerful single-cell RNA sequencing using mcSCRB-seq. Nat Commun 9, 2937.

Barron, M. and Li, J., 2016. Identifying and removing the cell-cycle effect from single-cell RNA-Sequencing data. Sci Rep 6, 33892.

Benz, P.M., Ding, Y., Stingl, H., Loot, A.E., Zink, J., Wittig, I., Popp, R. and Fleming, I., 2020. AKAP12 deficiency impairs VEGF-induced endothelial cell migration and sprouting. Acta Physiol (Oxf) 228, e13325.

Biros, E., Moran, C.S., Rush, C.M., Gäbel, G., Schreurs, C., Lindeman, J.H., Walker, P.J., Nataatmadja, M., West, M., Holdt, L.M., Hinterseher, I., Pilarsky, C. and Golledge, J., 2014. Differential gene expression in the proximal neck of human abdominal aortic aneurysm. Atherosclerosis 233, 211-218.

Biswas, L., Farhan, F., Reilly, J., Bartholomew, C. and Shu, X., 2018. TSPO Ligands Promote Cholesterol Efflux and Suppress Oxidative Stress and Inflammation in Choroidal Endothelial Cells. Int J Mol Sci 19, 3740.

Burgess, D.J., 2019. Spatial transcriptomics coming of age. Nat Rev Genet 20, 317.

Busch, A., Eken, S.M. and Maegdefessel, L., 2016. Prospective and therapeutic screening value of non-coding RNA as biomarkers in cardiovascular disease. Ann Transl Med 4, 236.

Butler, A., Hoffman, P., Smibert, P., Papalexi, E. and Satija, R., 2018. Integrating single-cell transcriptomic data across different conditions, technologies, and species. Nat Biotechnol 36, 411-420.

Cao, J., Packer, J.S., Ramani, V., Cusanovich, D.A., Huynh, C., Daza, R., Qiu, X., Lee, C., Furlan, S.N., Steemers, F.J., Adey, A., Waterston, R.H., Trapnell, C. and Shendure, J., 2017. Comprehensive single-cell transcriptional profiling of a multicellular organism. Science 357, 661-667.

Chaudhry, F., Isherwood, J., Bawa, T., Patel, D., Gurdziel, K., Lanfear, D.E., Ruden, D.M. and Levy, P.D., 2019. Single-Cell RNA Sequencing of the Cardiovascular System: New Looks for Old Diseases. Front Cardiovasc Med 6, 173.

Chavkin, N.W. and Hirschi, K.K., 2020. Single Cell Analysis in Vascular Biology. Front Cardiovasc Med 7, 42.

Chen, E.Y., Tan, C.M., Kou, Y., Duan, Q., Wang, Z., Meirelles, G.V., Clark, N.R. and Ma'ayan, A., 2013. Enrichr: interactive and collaborative HTML5 gene list enrichment analysis tool. BMC Bioinform 14, 128.

Chen, Z.-g., Tan, S.-p., Diao, Y.-p., Wu, Z.-y., Miao, Y.-q. and Li, Y.-j., 2019. The long-term outcomes of open and endovascular repair for abdominal aortic aneurysm: A meta-analysis. Asian J Surg 42, 899-906.

Cheng, C., Tempel, D., Den Dekker, W.K., Haasdijk, R., Chrifi, I., Bos, F.L., Wagtmans, K., van de Kamp, E.H., Blonden, L., Biessen, E.A., Moll, F., Pasterkamp, G., Serruys, P.W., Schulte-Merker, S. and Duckers, H.J., 2011. Ets2 determines the inflammatory state of endothelial cells in advanced atherosclerotic lesions. Circ Res 109, 382-395.

Cheng, C.K., Bakar, H.A., Gollasch, M. and Huang, Y., 2018. Perivascular Adipose Tissue: the Sixth Man of the Cardiovascular System. Cardiovasc Drugs Ther 32, 481-502.

Cochain, C., Vafadarnejad, E., Arampatzi, P., Pelisek, J., Winkels, H., Ley, K., Wolf, D., Saliba, A.E. and Zernecke, A., 2018. Single-Cell RNA-Seq Reveals the Transcriptional Landscape and Heterogeneity of Aortic Macrophages in Murine Atherosclerosis. Circ Res 122, 1661-1674.

Coen, M., Gabbiani, G. and Bochaton-Piallat, M.L., 2011. Myofibroblast-mediated adventitial remodeling: an underestimated player in arterial pathology. Arterioscler Thromb Vasc Biol 31, 2391-2396.

Dallinga, M.G., Habani, Y.I., Kayser, R.P., Van Noorden, C.J.F., Klaassen, I. and Schlingemann, R.O., 2020. IGF-binding proteins 3 and 4 are regulators of sprouting angiogenesis. Mol Biol Rep 47, 2561-2572.

de Kanter, J.K., Lijnzaad, P., Candelli, T., Margaritis, T. and Holstege, F.C.P., 2019. CHETAH: a selective, hierarchical cell type identification method for single-cell RNA sequencing. Nucleic Acids Res 47, e95.

Dias-Neto, M., Meekel, J.P., van Schaik, T.G., Hoozemans, J., Sousa-Nunes, F., Henriques-Coelho, T., Lely, R.J., Wisselink, W., Blankensteijn, J.D. and Yeung, K.K., 2018. High Density of Periaortic Adipose Tissue in Abdominal Aortic Aneurysm. Eur J Vasc Endovasc Surg 56, 663-671.

Dobnikar, L., Taylor, A.L., Chappell, J., Oldach, P., Harman, J.L., Oerton, E., Dzierzak, E., Bennett, M.R., Spivakov, M. and Jørgensen, H.F., 2018. Disease-relevant transcriptional signatures identified in individual smooth muscle cells from healthy mouse vessels. Nat Commun 9, 4567.

Domingues, A., Boisson-Vidal, C., Marquet de Rouge, P., Dizier, B., Sadoine, J., Mignon, V., Vessières, E., Henrion, D., Escriou, V., Bigey, P., Chaussain, C., Smadja, D.M. and Nivet-Antoine, V., 2020. Targeting endothelial thioredoxin-interacting protein (TXNIP) protects from metabolic disorder-related impairment of vascular function and post-ischemic revascularisation. Angiogenesis 23, 249-264.

Dubost, C., Allary, M. and Oeconomos, N., 1951. Treatment of aortic aneurysms; removal of the aneurysm; re-establishment of continuity by grafts of preserved human aorta. Memoires. Academie de chirurgie (France) 77, 381-383.

Eckstein, H.-H. and Maegdefessel, L., 2019. Linking obesity with abdominal aortic aneurysm development. Eur Heart J, ehz882.

Eng, C.L., Lawson, M., Zhu, Q., Dries, R., Koulena, N., Takei, Y., Yun, J., Cronin, C., Karp, C., Yuan, G.C. and Cai, L., 2019. Transcriptome-scale super-resolved imaging in tissues by RNA seqFISH. Nature 568, 235-239.

Fernandez, D.M., Rahman, A.H., Fernandez, N.F., Chudnovskiy, A., Amir, E.D., Amadori, L., Khan, N.S., Wong, C.K., Shamailova, R., Hill, C.A., Wang, Z., Remark, R., Li, J.R., Pina, C., Faries, C., Awad, A.J., Moss, N., Bjorkegren, J.L.M., Kim-Schulze, S., Gnjatic, S., Ma'ayan, A., Mocco, J., Faries, P., Merad, M. and Giannarelli, C., 2019. Single-cell immune landscape of human atherosclerotic plaques. Nat Med 25, 1576-1588.

Foley, J.W., Zhu, C., Jolivet, P., Zhu, S.X., Lu, P., Meaney, M.J. and West, R.B., 2019. Gene expression profiling of single cells from archival tissue with laser-capture microdissection and Smart-3SEQ. Genome Res 29, 1816-1825.

Fürth, D., Hatini, V. and Lee, J.H., 2019. In Situ Transcriptome Accessibility Sequencing (INSTA-seq). bioRxiv, 722819.

Gäbel, G., Northoff, B.H., Weinzierl, I., Ludwig, S., Hinterseher, I., Wilfert, W., Teupser, D., Doderer, S.A., Bergert, H., Schönleben, F., Lindeman, J.H.N. and Holdt, L.M., 2017. Molecular Fingerprint for Terminal Abdominal Aortic Aneurysm Disease. J Am Heart Assoc 6, e006798.

Garalde, D.R., Snell, E.A., Jachimowicz, D., Sipos, B., Lloyd, J.H., Bruce, M., Pantic, N., Admassu, T., James, P., Warland, A., Jordan, M., Ciccone, J., Serra, S., Keenan, J., Martin, S., McNeill, L., Wallace, E.J., Jayasinghe, L., Wright, C., Blasco, J., Young, S., Brocklebank, D., Juul, S., Clarke, J., Heron, A.J. and Turner, D.J., 2018. Highly parallel direct RNA sequencing on an array of nanopores. Nat Methods 15, 201-206.

García-Villegas, R., López-Alvarez, L.E., Arni, S., Rosenbaum, T. and Morales, M.A., 2009. Identification and functional characterization of the promoter of the mouse sodium-activated sodium channel Na(x) gene (Scn7a). J Neurosci Res 87, 2509-19.

Golledge, J., 2019. Abdominal aortic aneurysm: update on pathogenesis and medical treatments. Nat Rev Cardiol 16, 225-242.

Golledge, J., Pinchbeck, J., Tomee, S.M., Rowbotham, S.E., Singh, T.P., Moxon, J.V., Jenkins, J.S., Lindeman, J.H., Dalman, R.L., McDonnell, L., Fitridge, R., Morris, D.R. and Investigators, f.t.T., 2020. Efficacy of Telmisartan to Slow Growth of Small Abdominal Aortic Aneurysms: A Randomized Clinical Trial. JAMA Cardiology, Aug 26, e203524.

Gu, W., Nowak, W.N., Xie, Y., Le Bras, A., Hu, Y., Deng, J., Issa Bhaloo, S., Lu, Y., Yuan, H., Fidanis, E., Saxena, A., Kanno, T., Mason, A.J., Dulak, J., Cai, J. and Xu, Q., 2019. Single-Cell RNA-Sequencing and Metabolomics Analyses Reveal the Contribution of Perivascular Adipose Tissue Stem Cells to Vascular Remodeling. Arterioscler Thromb Vasc Biol 39, 2049-2066.

Hafemeister, C. and Satija, R., 2019. Normalization and variance stabilization of single-cell RNA-seq data using regularized negative binomial regression. Genome Biol 20, 296.

Hagemann-Jensen, M., Ziegenhain, C., Chen, P., Ramsköld, D., Hendriks, G.-J., Larsson, A.J.M., Faridani, O.R. and Sandberg, R., 2019. Single-cell RNA counting at allele- and isoform-resolution using Smart-seq3. bioRxiv, 817924.

Hashimshony, T., Senderovich, N., Avital, G., Klochendler, A., de Leeuw, Y., Anavy, L., Gennert, D., Li, S., Livak, K.J., Rozenblatt-Rosen, O., Dor, Y., Regev, A. and Yanai, I., 2016. CEL-Seq2: sensitive highly-multiplexed single-cell RNA-Seq. Genome Biol 17, 77.

Hashimshony, T., Wagner, F., Sher, N. and Yanai, I., 2012. CEL-Seq: single-cell RNA-Seq by multiplexed linear amplification. Cell Rep 2, 666-673.

Hayashi, T., Ozaki, H., Sasagawa, Y., Umeda, M., Danno, H. and Nikaido, I., 2018. Single-cell full-length total RNA sequencing uncovers dynamics of recursive splicing and enhancer RNAs. Nat

Commun 9, 619.

Helsinki, W.M.A.d.o., 1997. World Medical Association declaration of Helsinki.Recommendations guiding physicians in biomedical research involving human subjects. JAMA 277, 925-926.

Hoober, J.K., Eggink, L.L. and Cote, R., 2019. Stories From the Dendritic Cell Guardhouse. Front Immunol 10, 2880.

Islam, S., Kjallquist, U., Moliner, A., Zajac, P., Fan, J.B., Lonnerberg, P. and Linnarsson, S., 2012. Highly multiplexed and strand-specific single-cell RNA 5' end sequencing. Nat Protoc 7, 813-828.

Jaitin, D.A., Kenigsberg, E., Keren-Shaul, H., Elefant, N., Paul, F., Zaretsky, I., Mildner, A., Cohen, N., Jung, S., Tanay, A. and Amit, I., 2014. Massively parallel single-cell RNA-seq for marker-free decomposition of tissues into cell types. Science 343, 776-779.

Kalluri, A.S., Vellarikkal, S.K., Edelman, E.R., Nguyen, L., Subramanian, A., Ellinor, P.T., Regev, A., Kathiresan, S. and Gupta, R.M., 2019. Single-Cell Analysis of the Normal Mouse Aorta Reveals Functionally Distinct Endothelial Cell Populations. Circulation 140, 147-163.

Kaur, H., Carvalho, J., Looso, M., Singh, P., Chennupati, R., Preussner, J., Günther, S., Albarrán-Juárez, J., Tischner, D., Classen, S., Offermanns, S. and Wettschureck, N., 2017. Single-cell profiling reveals heterogeneity and functional patterning of GPCR expression in the vascular system. Nat Commun 8, 15700.

Kiselev, V.Y., Yiu, A. and Hemberg, M., 2018. scmap: projection of single-cell RNA-seq data across data sets. Nat Methods 15, 359-362.

Klein, A.M., Mazutis, L., Akartuna, I., Tallapragada, N., Veres, A., Li, V., Peshkin, L., Weitz, D.A. and Kirschner, M.W., 2015. Droplet barcoding for single-cell transcriptomics applied to embryonic stem cells. Cell 161, 1187-1201.

Krausgruber, T., Fortelny, N., Fife-Gernedl, V., Senekowitsch, M., Schuster, L.C., Lercher, A., Nemc, A., Schmidl, C., Rendeiro, A.F., Bergthaler, A. and Bock, C., 2020. Structural cells are key regulators of organ-specific immune responses. Nature 583, 296-302.

Kugo, H., Moriyama, T. and Zaima, N., 2019. The role of perivascular adipose tissue in the appearance of ectopic adipocytes in the abdominal aortic aneurysmal wall. Adipocyte 8, 229-239.

Kuleshov, M.V., Jones, M.R., Rouillard, A.D., Fernandez, N.F., Duan, Q., Wang, Z., Koplev, S., Jenkins, S.L., Jagodnik, K.M., Lachmann, A., McDermott, M.G., Monteiro, C.D., Gundersen, G.W. and Ma'ayan, A., 2016. Enrichr: a comprehensive gene set enrichment analysis web server 2016 update. Nucleic Acids Res 44, W90-97.

Kumar, S., Boon, R.A., Maegdefessel, L., Dimmeler, S. and Jo, H., 2019. Role of Noncoding RNAs in the Pathogenesis of Abdominal Aortic Aneurysm. Circ Res 124, 619-630.

Kushwaha, R., Mishra, J., Gupta, A.P., Gupta, K., Vishwakarma, J., Chattopadhyay, N., Gayen, J.R., Kamthan, M. and Bandyopadhyay, S., 2019. Rosiglitazone up-regulates glial fibrillary acidic protein via HB-EGF secreted from astrocytes and neurons through PPARγ pathway and reduces apoptosis in high-fat diet-fed mice. J Neurochem 149, 679-698.

Kuwabara, J.T. and Tallquist, M.D., 2017. Tracking Adventitial Fibroblast Contribution to Disease: A Review of Current Methods to Identify Resident Fibroblasts. Arterioscler Thromb Vasc Biol 37, 1598-1607.

Lafzi, A., Moutinho, C., Picelli, S. and Heyn, H., 2018. Tutorial: guidelines for the experimental design of single-cell RNA sequencing studies. Nat Protoc 13, 2742-2757.

Lagarde, J., Uszczynska-Ratajczak, B., Carbonell, S., Perez-Lluch, S., Abad, A., Davis, C., Gingeras, T.R.,

Frankish, A., Harrow, J., Guigo, R. and Johnson, R., 2017. High-throughput annotation of full-length long noncoding RNAs with capture long-read sequencing. Nat Genet 49, 1731-1740.

Lamas Bervejillo, M., Bonanata, J., Franchini, G.R., Richeri, A., Marqués, J.M., Freeman, B.A., Schopfer, F.J., Coitiño, E.L., Córsico, B., Rubbo, H. and Ferreira, A.M., 2020. A FABP4-PPARγ signaling axis regulates human monocyte responses to electrophilic fatty acid nitroalkenes. Redox Biol 29, 101376.

Lambert, J., Makin, K., Akbareian, S., Johnson, R., Alghamdi, A.A.A., Robinson, S.D. and Edwards, D.R., 2020. ADAMTS-1 and syndecan-4 intersect in the regulation of cell migration and angiogenesis. J Cell Sci 133, jcs235762.

Lao, K.Q., Tang, F., Barbacioru, C., Wang, Y., Nordman, E., Lee, C., Xu, N., Wang, X., Tuch, B., Bodeau, J., Siddiqui, A. and Surani, M.A., 2009. mRNA-sequencing whole transcriptome analysis of a single cell on the SOLiD system. J Biomol Tech 20, 266-271.

LeBleu, V.S. and Neilson, E.G., 2020. Origin and functional heterogeneity of fibroblasts. FASEB J 34, 3519-3536.

Lederle, F.A., Freischlag, J.A., Kyriakides, T.C., Matsumura, J.S., Padberg, F.T., Kohler, T.R., Kougias, P., Jean-Claude, J.M., Cikrit, D.F. and Swanson, K.M., 2012. Long-Term Comparison of Endovascular and Open Repair of Abdominal Aortic Aneurysm. N Engl J Med 367, 1988-1997.

Leeper, N.J. and Maegdefessel, L., 2018. Non-coding RNAs: key regulators of smooth muscle cell fate in vascular disease. Cardiovasc Res 114, 611-621.

Li, D.Y., Busch, A., Jin, H., Chernogubova, E., Pelisek, J., Karlsson, J., Sennblad, B., Liu, S., Lao, S., Hofmann, P., Bäcklund, A., Eken, S.M., Roy, J., Eriksson, P., Dacken, B., Ramanujam, D., Dueck, A., Engelhardt, S., Boon, R.A., Eckstein, H.H., Spin, J.M., Tsao, P.S. and Maegdefessel, L., 2018. H19 Induces Abdominal Aortic Aneurysm Development and Progression. Circulation 138, 1551-1568.

Lin, A., Dey, D., Wong, D.T.L. and Nerlekar, N., 2019. Perivascular Adipose Tissue and Coronary Atherosclerosis: from Biology to Imaging Phenotyping. Curr Atheroscler Rep 21, 47.

Liu, C.L., Ren, J., Wang, Y., Zhang, X., Sukhova, G.K., Liao, M., Santos, M., Luo, S., Yang, D., Xia, M., Inouye, K., Hotamisligil, G.S., Lu, G., Upchurch, G.R., Libby, P., Guo, J., Zhang, J. and Shi, G.P., 2020. Adipocytes promote interleukin-18 binding to its receptors during abdominal aortic aneurysm formation in mice. Eur Heart J 41, 2456-2468.

Liu, X., Chen, W., Li, W., Li, Y., Priest, J.R., Zhou, B., Wang, J. and Zhou, Z., 2019. Single-Cell RNA-Seq of the Developing Cardiac Outflow Tract Reveals Convergent Development of the Vascular Smooth Muscle Cells. Cell Rep 28, 1346-1361.e4.

Looyenga, B.D., Resau, J. and MacKeigan, J.P., 2013. Cytokine receptor-like factor 1 (CRLF1) protects against 6-hydroxydopamine toxicity independent of the gp130/JAK signaling pathway. PLoS One 8, e66548.

Lysgaard Poulsen, J., Stubbe, J. and Lindholt, J.S., 2016. Animal Models Used to Explore Abdominal Aortic Aneurysms: A Systematic Review. Eur J Vasc Endovasc Surg 52, 487-499.

Macosko, E.Z., Basu, A., Satija, R., Nemesh, J., Shekhar, K., Goldman, M., Tirosh, I., Bialas, A.R., Kamitaki, N., Martersteck, E.M., Trombetta, J.J., Weitz, D.A., Sanes, J.R., Shalek, A.K., Regev, A. and McCarroll, S.A., 2015. Highly Parallel Genome-wide Expression Profiling of Individual Cells Using Nanoliter Droplets. Cell 161, 1202-1214.

Maegdefessel, L., Spin, J.M., Adam, M., Raaz, U., Toh, R., Nakagami, F. and Tsao, P.S., 2013. Micromanaging abdominal aortic aneurysms. Int J Mol Sci 14, 14374-14394.

Maegdefessel, L., Spin, J.M., Raaz, U., Eken, S.M., Toh, R., Azuma, J., Adam, M., Nagakami, F., Heymann, H.M., Chernugobova, E., Jin, H., Roy, J., Hultgren, R., Caidahl, K., Schrepfer, S., Hamsten, A., Eriksson, P., McConnell, M.V., Dalman, R.L. and Tsao, P.S., 2014. miR-24 limits aortic vascular inflammation and murine abdominal aneurysm development. Nature Commun 5, 5214.

Maguire, E.M., Pearce, S.W.A., Xiao, R., Oo, A.Y. and Xiao, Q., 2019. Matrix Metalloproteinase in Abdominal Aortic Aneurysm and Aortic Dissection. Pharmaceuticals (Basel) 12,118.

Makaloski, V., Kölbel, T., Rohlffs, F., Behrendt, C.A., Law, Y., Debus, E.S. and Tsilimparis, N., 2018. Early Outcomes After Branched and Fenestrated Endovascular Aortic Repair in Octogenarians. Eur J Vasc Endovasc Surg 56, 818-825.

Marzelle, J., Presles, E., Becquemin, J.P. and participants, W.t., 2015. Results and factors affecting early outcome of fenestrated and/or branched stent grafts for aortic aneurysms: a multicenter prospective study. Ann Surg 261, 197-206.

Murphy, P.A. and Hynes, R.O., 2014. Alternative splicing of endothelial fibronectin is induced by disturbed hemodynamics and protects against hemorrhage of the vessel wall. Arterioscler Thromb Vasc Biol 34, 2042-2050.

Newby, D., Forsythe, R., McBride, O., Robson, J., Vesey, A., Chalmers, R., Burns, P., Garden, O.J., Semple, S., Dweck, M., Gray, C., MacGillivray, T., Wang, C., Koutraki, Y.G., Mitchard, N., Cooper, A., Beek, E.v., McKillop, G., Ho, W., Fraser, L., Cuthbert, H., Hoskins, P., Doyle, B., Conlisk, N., Stuart, W., Berry, C., Roditi, G., Murdoch, L., Holdsworth, R., Scott, E., Milne, L., Strachan, F., Wee, F., Oatey, K., Graham, C., Murray, G., Milne, G., Bucukoglu, M., Goodman, K., Kaczynski, J., Shah, A., Tambyraja, A., Brittenden, J., Houston, G., Lambie, R. and Norrie, J., 2017. Aortic Wall Inflammation Predicts Abdominal Aortic Aneurysm Expansion, Rupture, and Need for Surgical Repair. Circulation 136, 787-797.

Nitti, M., Piras, S., Brondolo, L., Marinari, U.M., Pronzato, M.A. and Furfaro, A.L., 2018. Heme Oxygenase 1 in the Nervous System: Does It Favor Neuronal Cell Survival or Induce Neurodegeneration? Int J Mol Sci 19,2260.

Oikari, L.E., Okolicsanyi, R.K., Qin, A., Yu, C., Griffiths, L.R. and Haupt, L.M., 2016. Cell surface heparan sulfate proteoglycans as novel markers of human neural stem cell fate determination. Stem Cell Res 16, 92-104.

Pan, H., Xue, C., Auerbach, B.J., Fan, J., Bashore, A.C., Cui, J., Yang, D.Y., Trignano, S.B., Liu, W., Shi, J., Ihuegbu, C.O., Bush, E.C., Worley, J., Vlahos, L., Laise, P., Solomon, R.A., Connolly, E.S., Califano, A., Sims, P.A., Zhang, H., Li, M. and Reilly, M.P., 2020. Single-Cell Genomics Reveals a Novel Cell State During Smooth Muscle Cell Phenotypic Switching and Potential Therapeutic Targets for Atherosclerosis in Mouse and Human. Circulation 142, 2060-2075.

Parkinson, F., Ferguson, S., Lewis, P., Williams, I.M., Twine, C.P. and South East Wales Vascular, N., 2015. Rupture rates of untreated large abdominal aortic aneurysms in patients unfit for elective repair. J Vasc Surg 61, 1606-1612.

Parodi, J.C., Palmaz, J.C. and Barone, H.D., 1991. Transfemoral Intraluminal Graft Implantation for Abdominal Aortic Aneurysms. Ann Vasc Surg 5, 491-499.

Patel, R., Sweeting, M.J., Powell, J.T., Greenhalgh, R.M. and investigators, E.t., 2016. Endovascular versus open repair of abdominal aortic aneurysm in 15-years' follow-up of the UK

endovascular aneurysm repair trial 1 (EVAR trial 1): a randomised controlled trial. Lancet 388, 2366-2374.

Pedroza, A.J., Tashima, Y., Shad, R., Cheng, P., Wirka, R., Churovich, S., Nakamura, K., Yokoyama, N., Cui, J.Z., Iosef, C., Hiesinger, W., Quertermous, T. and Fischbein, M.P., 2020. Single-Cell Transcriptomic Profiling of Vascular Smooth Muscle Cell Phenotype Modulation in Marfan Syndrome Aortic Aneurysm. Arterioscler Thromb Vasc Biol 40, 2195-2211.

Pelisek, J., Hegenloh, R., Bauer, S., Metschl, S., Pauli, J., Glukha, N., Busch, A., Reutersberg, B., Kallmayer, M., Trenner, M., Wendorff, H., Tsantilas, P., Schmid, S., Knappich, C., Schaeffer, C., Stadlbauer, T., Biro, G., Wertern, U., Meisner, F., Stoklasa, K., Menges, A.L., Radu, O., Dallmann-Sieber, S., Karlas, A., Knipfer, E., Reeps, C., Zimmermann, A., Maegdefessel, L. and Eckstein, H.H., 2019. Biobanking: Objectives, Requirements, and Future Challenges-Experiences from the Munich Vascular Biobank. J Clin Med 8,251.

Pellicani, R., Poletto, E., Andreuzzi, E., Paulitti, A., Doliana, R., Bizzotto, D., Braghetta, P., Colladel, R., Tarticchio, G., Sabatelli, P., Bucciotti, F., Bressan, G., Iozzo, R.V., Colombatti, A., Bonaldo, P. and Mongiat, M., 2020. Multimerin-2 maintains vascular stability and permeability. Matrix Biol 87, 11-25.

Piacentini, L., Werba, J.P., Bono, E., Saccu, C., Tremoli, E., Spirito, R. and Colombo, G.I., 2019. Genome-Wide Expression Profiling Unveils Autoimmune Response Signatures in the Perivascular Adipose Tissue of Abdominal Aortic Aneurysm. Arterioscler Thromb Vasc Biol 39, 237-249.

Picelli, S., Faridani, O.R., Bjorklund, A.K., Winberg, G., Sagasser, S. and Sandberg, R., 2014. Full-length RNA-seq from single cells using Smart-seq2. Nat Protoc 9, 171-181.

Plana, E., Oto, J., Medina, P., Fernández-Pardo, Á. and Miralles, M., 2020. Novel contributions of neutrophils in the pathogenesis of abdominal aortic aneurysm, the role of neutrophil extracellular traps: A systematic review. Thromb Res 194, 200-208.

Pliner, H.A., Shendure, J. and Trapnell, C., 2019. Supervised classification enables rapid annotation of cell atlases. Nat Methods 16, 983-986.

Powell, J.T., Sweeting, M.J., Ulug, P., Blankensteijn, J.D., Lederle, F.A., Becquemin, J.P., Greenhalgh, R.M., Evar, D.O. and Trialists, A.C.E., 2017. Meta-analysis of individual-patient data from EVAR-1, DREAM, OVER and ACE trials comparing outcomes of endovascular or open repair for abdominal aortic aneurysm over 5 years. The British journal of surgery 104, 166-178.

Pronk, M.C.A., van Bezu, J.S.M., van Nieuw Amerongen, G.P., van Hinsbergh, V.W.M. and Hordijk, P.L., 2019. RhoA, RhoB and RhoC differentially regulate endothelial barrier function. Small GTPases 10, 466-484.

Robbins, C.S., Hilgendorf, I., Weber, G.F., Theurl, I., Iwamoto, Y., Figueiredo, J.L., Gorbatov, R., Sukhova, G.K., Gerhardt, L.M., Smyth, D., Zavitz, C.C., Shikatani, E.A., Parsons, M., van Rooijen, N., Lin, H.Y., Husain, M., Libby, P., Nahrendorf, M., Weissleder, R. and Swirski, F.K., 2013. Local proliferation dominates lesional macrophage accumulation in atherosclerosis. Nat Med 19, 1166-1172.

Rodemerk, J., Junker, A., Chen, B., Pierscianek, D., Dammann, P., Darkwah Oppong, M., Radbruch, A., Forsting, M., Maderwald, S., Quick, H.H., Zhu, Y., Jabbarli, R., Sure, U. and Wrede, K.H., 2020. Pathophysiology of Intracranial Aneurysms: COX-2 Expression, Iron Deposition in Aneurysm Wall, and Correlation With Magnetic Resonance Imaging. Stroke 51, 2505-2513.

Rodriques, S.G., Stickels, R.R., Goeva, A., Martin, C.A., Murray, E., Vanderburg, C.R., Welch, J., Chen,

L.M., Chen, F. and Macosko, E.Z., 2019. Slide-seq: A scalable technology for measuring genome-wide expression at high spatial resolution. Science 363, 1463-1467.

Rosenberg, A.B., Roco, C.M., Muscat, R.A., Kuchina, A., Sample, P., Yao, Z., Graybuck, L.T., Peeler, D.J., Mukherjee, S., Chen, W., Pun, S.H., Sellers, D.L., Tasic, B. and Seelig, G., 2018. Single-cell profiling of the developing mouse brain and spinal cord with split-pool barcoding. Science 360, 176-182.

Sabater-Lleal, M., Huffman, J.E., de Vries, P.S., Marten, J., Mastrangelo, M.A., Song, C., Pankratz, N., Ward-Caviness, C.K., Yanek, L.R., Trompet, S., Delgado, G.E., Guo, X., Bartz, T.M., Martinez-Perez, A., Germain, M., de Haan, H.G., Ozel, A.B., Polasek, O., Smith, A.V., Eicher, J.D., Reiner, A.P., Tang, W., Davies, N.M., Stott, D.J., Rotter, J.I., Tofler, G.H., Boerwinkle, E., de Maat, M.P.M., Kleber, M.E., Welsh, P., Brody, J.A., Chen, M.H., Vaidya, D., Soria, J.M., Suchon, P., van Hylckama Vlieg, A., Desch, K.C., Kolcic, I., Joshi, P.K., Launer, L.J., Harris, T.B., Campbell, H., Rudan, I., Becker, D.M., Li, J.Z., Rivadeneira, F., Uitterlinden, A.G., Hofman, A., Franco, O.H., Cushman, M., Psaty, B.M., Morange, P.E., McKnight, B., Chong, M.R., Fernandez-Cadenas, I., Rosand, J., Lindgren, A., Gudnason, V., Wilson, J.F., Hayward, C., Ginsburg, D., Fornage, M., Rosendaal, F.R., Souto, J.C., Becker, L.C., Jenny, N.S., März, W., Jukema, J.W., Dehghan, A., Trégouët, D.A., Morrison, A.C., Johnson, A.D., O'Donnell, C.J., Strachan, D.P., Lowenstein, C.J. and Smith, N.L., 2019. Genome-Wide Association Transethnic Meta-Analyses Identifies Novel Associations Regulating Coagulation Factor VIII and von Willebrand Factor Plasma Levels. Circulation 139, 620-635.

Sagan, A., Mikolajczyk, T.P., Mrowiecki, W., MacRitchie, N., Daly, K., Meldrum, A., Migliarino, S., Delles, C., Urbanski, K., Filip, G., Kapelak, B., Maffia, P., Touyz, R. and Guzik, T.J., 2019. T Cells Are Dominant Population in Human Abdominal Aortic Aneurysms and Their Infiltration in the Perivascular Tissue Correlates With Disease Severity. Front Immunol 10, 1979.

Sahraeian, S.M.E., Mohiyuddin, M., Sebra, R., Tilgner, H., Afshar, P.T., Au, K.F., Bani Asadi, N., Gerstein, M.B., Wong, W.H., Snyder, M.P., Schadt, E. and Lam, H.Y.K., 2017. Gaining comprehensive biological insight into the transcriptome by performing a broad-spectrum RNA-seq analysis. Nat Commun 8, 59.

Salomon, R., Kaczorowski, D., Valdes-Mora, F., Nordon, R.E., Neild, A., Farbehi, N., Bartonicek, N. and Gallego-Ortega, D., 2019. Droplet-based single cell RNAseq tools: a practical guide. Lab Chip 19, 1706-1727.

Sampson, U.K.A., Norman, P.E., Fowkes, F.G.R., Aboyans, V., Song, Y., Harrell, F.E., Jr., Forouzanfar, M.H., Naghavi, M., Denenberg, J.O., McDermott, M.M., Criqui, M.H., Mensah, G.A., Ezzati, M. and Murray, C., 2014. Estimation of global and regional incidence and prevalence of abdominal aortic aneurysms 1990 to 2010. Global heart 9, 159-170.

Sasagawa, Y., Danno, H., Takada, H., Ebisawa, M., Tanaka, K., Hayashi, T., Kurisaki, A. and Nikaido, I., 2018. Quartz-Seq2: a high-throughput single-cell RNA-sequencing method that effectively uses limited sequence reads. Genome Biol 19, 29.

Sasagawa, Y., Nikaido, I., Hayashi, T., Danno, H., Uno, K.D., Imai, T. and Ueda, H.R., 2013. Quartz-Seq: a highly reproducible and sensitive single-cell RNA sequencing method, reveals non-genetic gene-expression heterogeneity. Genome Biol 14, R31.

Schott, J., Reitter, S., Philipp, J., Haneke, K., Schäfer, H. and Stoecklin, G., 2014. Translational regulation of specific mRNAs controls feedback inhibition and survival during macrophage activation. PLoS Genet 10, e1004368.

Shao, X., Liao, J., Lu, X., Xue, R., Ai, N. and Fan, X., 2020. scCATCH: Automatic Annotation on Cell Types of Clusters from Single-Cell RNA Sequencing Data. iScience 23, 100882.

Silvestre-Roig, C., Braster, Q., Wichapong, K., Lee, E.Y., Teulon, J.M., Berrebeh, N., Winter, J., Adrover, J.M., Santos, G.S., Froese, A., Lemnitzer, P., Ortega-Gómez, A., Chevre, R., Marschner, J., Schumski, A., Winter, C., Perez-Olivares, L., Pan, C., Paulin, N., Schoufour, T., Hartwig, H., González-Ramos, S., Kamp, F., Megens, R.T.A., Mowen, K.A., Gunzer, M., Maegdefessel, L., Hackeng, T., Lutgens, E., Daemen, M., von Blume, J., Anders, H.J., Nikolaev, V.O., Pellequer, J.L., Weber, C., Hidalgo, A., Nicolaes, G.A.F., Wong, G.C.L. and Soehnlein, O., 2019. Externalized histone H4 orchestrates chronic inflammation by inducing lytic cell death. Nature 569, 236-240.

Soumillon, M., Cacchiarelli, D., Semrau, S., van Oudenaarden, A. and Mikkelsen, T.S., 2014. Characterization of directed differentiation by high-throughput single-cell RNA-Seq. bioRxiv, 003236.

Ståhl, P.L., Salmén, F., Vickovic, S., Lundmark, A., Navarro, J.F., Magnusson, J., Giacomello, S., Asp, M., Westholm, J.O., Huss, M., Mollbrink, A., Linnarsson, S., Codeluppi, S., Borg, Å., Pontén, F., Costea, P.I., Sahlén, P., Mulder, J., Bergmann, O., Lundeberg, J. and Frisén, J., 2016. Visualization and analysis of gene expression in tissue sections by spatial transcriptomics. Science 353, 78-82.

Stark, R., Grzelak, M. and Hadfield, J., 2019. RNA sequencing: the teenage years. Nat Rev Genet 20, 631-656.

Stuart, T., Butler, A., Hoffman, P., Hafemeister, C., Papalexi, E., Mauck, W.M., 3rd, Hao, Y., Stoeckius, M., Smibert, P. and Satija, R., 2019. Comprehensive Integration of Single-Cell Data. Cell 177, 1888-1902.e21.

Svensson, V., Vento-Tormo, R. and Teichmann, S.A., 2018. Exponential scaling of single-cell RNA-seq in the past decade. Nat Protoc 13, 599-604.

Tabib, T., Morse, C., Wang, T., Chen, W. and Lafyatis, R., 2018. SFRP2/DPP4 and FMO1/LSP1 Define Major Fibroblast Populations in Human Skin. J Invest Dermatol 138, 802-810.

Tang, F., Barbacioru, C., Wang, Y., Nordman, E., Lee, C., Xu, N., Wang, X., Bodeau, J., Tuch, B.B., Siddiqui, A., Lao, K. and Surani, M.A., 2009. mRNA-Seq whole-transcriptome analysis of a single cell. Nat Methods 6, 377-382.

Tillie, R., van Kuijk, K. and Sluimer, J.C., 2020. Fibroblasts in atherosclerosis: heterogeneous and plastic participants. Curr Opin Lipidol 31, 273-278.

Tinajero, M.G. and Gotlieb, A.I., 2020. Recent Developments in Vascular Adventitial Pathobiology: The Dynamic Adventitia as a Complex Regulator of Vascular Disease. Am J Pathol 190, 520-534.

van Kuijk, K., Kuppe, C., Betsholtz, C., Vanlandewijck, M., Kramann, R. and Sluimer, J.C., 2019. Heterogeneity and plasticity in healthy and atherosclerotic vasculature explored by single-cell sequencing. Cardiovasc Res 115, 1705-1715.

Vega de Céniga, M., Gómez, R., Estallo, L., de la Fuente, N., Viviens, B. and Barba, A., 2008. Analysis of Expansion Patterns in 4-4.9 cm Abdominal Aortic Aneurysms. Ann Vasc Surg 22, 37-44.

Verboom, K., Everaert, C., Bolduc, N., Livak, K.J., Yigit, N., Rombaut, D., Anckaert, J., Lee, S., Venø, M.T., Kjems, J., Speleman, F., Mestdagh, P. and Vandesompele, J., 2019. SMARTer single cell total RNA sequencing. Nucleic Acids Res 47, e93.

Wang, S., Song, R., Wang, Z., Jing, Z., Wang, S. and Ma, J., 2018. S100A8/A9 in Inflammation. Front

Immunol 9, 1298.

Wang, Y.J., Schug, J., Lin, J., Wang, Z., Kossenkov, A. and Kaestner, K.H., 2019. Comparative analysis of commercially available single-cell RNA sequencing platforms for their performance in complex human tissues. bioRxiv, 541433.

Wanhainen, A., Verzini, F., Van Herzeele, I., Allaire, E., Bown, M., Cohnert, T., Dick, F., van Herwaarden, J., Karkos, C., Koelemay, M., Kolbel, T., Loftus, I., Mani, K., Melissano, G., Powell, J., Szeberin, Z., Esvs Guidelines, C., de Borst, G.J., Chakfe, N., Debus, S., Hinchliffe, R., Kakkos, S., Koncar, I., Kolh, P., Lindholt, J.S., de Vega, M., Vermassen, F., Document, R., Bjorck, M., Cheng, S., Dalman, R., Davidovic, L., Donas, K., Earnshaw, J., Eckstein, H.H., Golledge, J., Haulon, S., Mastracci, T., Naylor, R., Ricco, J.B. and Verhagen, H., 2019. Editor's Choice - European Society for Vascular Surgery (ESVS) 2019 Clinical Practice Guidelines on the Management of Abdominal Aorto-iliac Artery Aneurysms. Eur J Vasc Endovasc Surg 57, 8-93.

Wei, S.T., Huang, Y.C., Hsieh, M.L., Lin, Y.J., Shyu, W.C., Chen, H.C. and Hsieh, C.H., 2020. Atypical chemokine receptor ACKR3/CXCR7 controls postnatal vasculogenesis and arterial specification by mesenchymal stem cells via Notch signaling. Cell Death Dis 11, 307.

Willemsen, L. and de Winther, M.P., 2020. Macrophage subsets in atherosclerosis as defined by single-cell technologies. J Pathol 250, 705-714.

Williams, J.W., Giannarelli, C., Rahman, A., Randolph, G.J. and Kovacic, J.C., 2018. Macrophage Biology, Classification, and Phenotype in Cardiovascular Disease: JACC Macrophage in CVD Series (Part 1). J Am Coll Cardiol 72, 2166-2180.

Williams, J.W., Winkels, H., Durant, C.P., Zaitsev, K., Ghosheh, Y. and Ley, K., 2020a. Single Cell RNA Sequencing in Atherosclerosis Research. Circ Res 126, 1112-1126.

Williams, J.W., Zaitsev, K., Kim, K.W., Ivanov, S., Saunders, B.T., Schrank, P.R., Kim, K., Elvington, A., Kim, S.H., Tucker, C.G., Wohltmann, M., Fife, B.T., Epelman, S., Artyomov, M.N., Lavine, K.J., Zinselmeyer, B.H., Choi, J.H. and Randolph, G.J., 2020b. Limited proliferation capacity of aortic intima resident macrophages requires monocyte recruitment for atherosclerotic plaque progression. Nat Immunol 21, 1194-1204.

Wilson, D.P., 2011. Vascular Smooth Muscle Structure and Function, in: Fitridge, R. and Thompson, M. (Eds.), Mechanisms of Vascular Disease: A Reference Book for Vascular Specialists. University of Adelaide Press, Adelaide (AU).

Wirka, R.C., Wagh, D., Paik, D.T., Pjanic, M., Nguyen, T., Miller, C.L., Kundu, R., Nagao, M., Coller, J., Koyano, T.K., Fong, R., Woo, Y.J., Liu, B., Montgomery, S.B., Wu, J.C., Zhu, K., Chang, R., Alamprese, M., Tallquist, M.D., Kim, J.B. and Quertermous, T., 2019. Atheroprotective roles of smooth muscle cell phenotypic modulation and the TCF21 disease gene as revealed by single-cell analysis. Nat Med 25, 1280-1289.

Wu, Z.-y., Trenner, M., Boon, R.A., Spin, J.M. and Maegdefessel, L., 2020. Long noncoding RNAs in key cellular processes involved in aortic aneurysms. Atherosclerosis 292, 112-118.

Wu, Z.Y., Chen, Z.G., Diao, Y.P., Sun, R., Liu, C.W., Chen, Y.X., Zheng, Y.H., Liu, B. and Li, Y.J., 2019a. Endovascular Repair of Complex Aortoiliac Aneurysm with the Sandwich Technique in Sixteen Patients. Ann Vasc Surg 54, 233-239.

Wu, Z.Y., Chen, Z.G., Ma, L., Diao, Y.P., Chen, Y.X., Liu, C.W., Zheng, Y.H., Liu, B. and Li, Y.J., 2017. Outcomes of Chimney and/or Periscope Techniques in the Endovascular Management of Complex Aortic Pathologies. Chin Med J (Engl) 130, 2095-2100.

Wu, Z.Y., Li, P., Wang, J.Y., Diao, Y.P., Chen, Z.G., Miao, Y.Q., Chang, Z.G., Zhang, H. and Li, Y.J., 2019b.

Aortic intimal intussusception during acute type B aortic dissection endovascular repair. Ann Transl Med 7, 700.

Yu, G. and He, Q.Y., 2016. ReactomePA: an R/Bioconductor package for reactome pathway analysis and visualization. Mol Biosyst 12, 477-479.

Yu, G., Wang, L.G., Han, Y. and He, Q.Y., 2012. clusterProfiler: an R package for comparing biological themes among gene clusters. Omics 16, 284-287.

Zernecke, A., Winkels, H., Cochain, C., Williams, J.W., Wolf, D., Soehnlein, O., Robbins, C.S., Monaco, C., Park, I., McNamara, C.A., Binder, C.J., Cybulsky, M.I., Scipione, C.A., Hedrick, C.C., Galkina, E.V., Kyaw, T., Ghosheh, Y., Dinh, H.Q. and Ley, K., 2020. Meta-Analysis of Leukocyte Diversity in Atherosclerotic Mouse Aortas. Circ Res 127, 402-426.

Zhang, A.W., O'Flanagan, C., Chavez, E.A., Lim, J.L.P., Ceglia, N., McPherson, A., Wiens, M., Walters, P., Chan, T., Hewitson, B., Lai, D., Mottok, A., Sarkozy, C., Chong, L., Aoki, T., Wang, X., Weng, A.P., McAlpine, J.N., Aparicio, S., Steidl, C., Campbell, K.R. and Shah, S.P., 2019a. Probabilistic cell-type assignment of single-cell RNA-seq for tumor microenvironment profiling. Nat Methods 16, 1007-1015.

Zhang, K., Yu, F., Zhu, J., Han, S., Chen, J., Wu, X., Chen, Y., Shen, T., Liao, J., Guo, W., Yang, X., Wang, R., Qian, Y., Yang, J., Cheng, L., Zhao, Y., Hui, C.C., Li, J., Peng, G., He, S., Jing, N. and Tang, K., 2020. Imbalance of Excitatory/Inhibitory Neuron Differentiation in Neurodevelopmental Disorders with an NR2F1 Point Mutation. Cell Rep 31, 107521.

Zhang, L., Lei, Y., Wang, Y. and Chen, X., 2018. Matrix projective synchronization for time-varying disturbed networks with uncertain nonlinear structures and different dimensional nodes. Neurocomputing 311, 11-23.

Zhang, Z., Zou, G., Chen, X., Lu, W., Liu, J., Zhai, S. and Qiao, G., 2019b. Knockdown of lncRNA PVT1 Inhibits Vascular Smooth Muscle Cell Apoptosis and Extracellular Matrix Disruption in a Murine Abdominal Aortic Aneurysm Model. Mol Cells 42, 218-227.

Zhao, G., Lu, H., Chang, Z., Zhao, Y., Zhu, T., Chang, L., Guo, Y., Garcia-Barrio, M.T., Chen, Y.E. and Zhang, J., 2020. Single cell RNA sequencing reveals the cellular heterogeneity of aneurysmal infrarenal abdominal aorta. Cardiovasc Res, cvaa214.

Zheng, G.X., Terry, J.M., Belgrader, P., Ryvkin, P., Bent, Z.W., Wilson, R., Ziraldo, S.B., Wheeler, T.D., McDermott, G.P., Zhu, J., Gregory, M.T., Shuga, J., Montesclaros, L., Underwood, J.G., Masquelier, D.A., Nishimura, S.Y., Schnall-Levin, M., Wyatt, P.W., Hindson, C.M., Bharadwaj, R., Wong, A., Ness, K.D., Beppu, L.W., Deeg, H.J., McFarland, C., Loeb, K.R., Valente, W.J., Ericson, N.G., Stevens, E.A., Radich, J.P., Mikkelsen, T.S., Hindson, B.J. and Bielas, J.H., 2017. Massively parallel digital transcriptional profiling of single cells. Nat Commun 8, 14049.

Ziegenhain, C., Vieth, B., Parekh, S., Reinius, B., Guillaumet-Adkins, A., Smets, M., Leonhardt, H., Heyn, H., Hellmann, I. and Enard, W., 2017. Comparative Analysis of Single-Cell RNA Sequencing Methods. Mol Cell 65, 631-643.e4.

8. SUPPLEMENT TABLES

Table S1. Estimation of the cell-barcode and UMIs in each library

	Non-dilated		Dilated	
	Self	Milt	Self	Milt
Estimated Number of Cells	559	414	280	437
Fraction Reads in Cells	71.3%	63.2%	74.2%	75.8%
Mean Reads per Cell	519,569	380,227	350,477	548,165
Median Genes per Cell	576	472	375	386
Total Genes Detected	23,768	18,984	17,356	21,678
Median UMI Counts per Cell	1,468	1,132	1,266	1,671
Sequencing Saturation	95.9%	93.7%	95.5%	96.4%

Table S2. Top ten markers in each cluster among the 15 clusters of all cells

Gene	p_val	avg_logFC	pct.1	pct.2	p_val_adj	cluster
MMP9	6.44E-29	1.673	0.308	0.034	9.37E-25	0
MMP12	4.70E-21	1.624	0.327	0.059	6.84E-17	0
FBP1	1.50E-15	1.617	0.271	0.058	2.19E-11	0
SPP1	8.68E-33	1.578	0.785	0.282	1.26E-28	0
AC020656.1	8.37E-12	1.507	0.299	0.094	1.22E-07	0
MT1G	8.73E-19	1.497	0.271	0.047	1.27E-14	0
LYZ	4.15E-22	1.471	0.72	0.323	6.04E-18	0
APOC1	3.09E-20	1.379	0.645	0.269	4.50E-16	0
MT1H	1.61E-15	1.294	0.215	0.034	2.34E-11	0
HK2	1.23E-13	1.260	0.262	0.062	1.79E-09	0
TNF	3.72E-27	2.404	0.414	0.071	5.41E-23	1
CCL20	1.28E-59	2.230	0.632	0.064	1.87E-55	1
IL1B	8.14E-50	1.995	0.69	0.104	1.18E-45	1
CXCL3	1.51E-52	1.973	0.77	0.134	2.20E-48	1
CD163	2.31E-35	1.774	0.667	0.158	3.36E-31	1
PHLDA1	8.07E-38	1.731	0.678	0.154	1.17E-33	1
TGFBI	5.13E-27	1.705	0.552	0.138	7.46E-23	1
EREG	2.33E-35	1.647	0.586	0.104	3.39E-31	1
LGMN	4.26E-23	1.604	0.575	0.167	6.20E-19	1
RRAD	7.35E-32	1.588	0.264	0.016	1.07E-27	1
SELENOP	1.60E-41	2.348	0.553	0.08	2.33E-37	2
C1QB	3.07E-42	1.997	0.718	0.149	4.47E-38	2
C1QC	1.39E-44	1.904	0.647	0.108	2.02E-40	2
C1QA	4.58E-30	1.728	0.659	0.168	6.67E-26	2
PLTP	6.35E-22	1.695	0.541	0.157	9.24E-18	2
FOLR2	9.81E-26	1.543	0.282	0.028	1.43E-21	2

LGMN	6.64E-19	1.428	0.541	0.171	9.67E-15	2
CCL18	3.01E-14	1.413	0.224	0.036	4.38E-10	2
RGS1	3.46E-14	1.372	0.506	0.189	5.03E-10	2
GPNMB	1.15E-17	1.359	0.624	0.237	1.67E-13	2
SPP1	6.09E-52	2.166	0.963	0.28	8.86E-48	3
MMP12	2.94E-66	1.829	0.617	0.041	4.28E-62	3
CTSB	4.16E-45	1.691	1	0.437	6.05E-41	3
RNASE1	9.86E-45	1.615	0.988	0.334	1.43E-40	3
SCD	3.64E-42	1.585	0.469	0.044	5.29E-38	3
CD36	3.61E-34	1.504	0.642	0.124	5.26E-30	3
FABP4	2.89E-34	1.439	0.432	0.047	4.20E-30	3
CSTB	6.56E-38	1.399	0.938	0.349	9.54E-34	3
CTSD	2.04E-36	1.370	0.951	0.336	2.97E-32	3
FTL	4.62E-34	1.339	1	0.929	6.72E-30	3
IL7R	5.80E-83	2.166	0.85	0.081	8.44E-79	4
CD2	6.85E-72	1.697	0.662	0.047	9.96E-68	4
CRYBG1	3.41E-76	1.691	0.788	0.075	4.97E-72	4
BCL11B	1.35E-87	1.622	0.788	0.052	1.96E-83	4
CNOT6L	5.69E-58	1.617	0.825	0.126	8.28E-54	4
SARAF	5.29E-40	1.521	0.912	0.3	7.69E-36	4
ITK	1.02E-92	1.504	0.625	0.021	1.48E-88	4
TSC22D3	3.22E-23	1.439	0.788	0.296	4.69E-19	4
TRBC2	1.41E-58	1.412	0.638	0.06	2.06E-54	4
TNFAIP3	2.58E-34	1.394	0.912	0.271	3.75E-30	4
IGKC	6.79E-20	6.243	0.646	0.246	9.88E-16	5
IGLC2	5.22E-09	5.709	0.443	0.207	7.59E-05	5
IGHG1	1.50E-38	5.702	0.38	0.031	2.18E-34	5
IGLC3	5.49E-20	5.605	0.405	0.085	7.99E-16	5
IGHG4	5.37E-16	5.526	0.329	0.067	7.82E-12	5
IGHG3	6.80E-40	5.522	0.519	0.069	9.89E-36	5
HBA1	3.28E-07	4.976	0.291	0.106	0.00476851	5
IGHG2	2.09E-47	4.656	0.354	0.015	3.04E-43	5
JCHAIN	2.65E-73	3.486	0.557	0.027	3.85E-69	5
IGHGP	2.23E-24	2.759	0.114	0	3.25E-20	5
CXCL14	1.31E-141	3.623	0.955	0.032	1.90E-137	6
FBLN1	1.24E-116	3.302	0.909	0.045	1.80E-112	6
PLA2G2A	3.52E-138	3.282	0.848	0.019	5.12E-134	6
C3	1.56E-115	2.980	0.97	0.058	2.27E-111	6
CCL2	6.41E-76	2.812	0.985	0.143	9.33E-72	6
HAS1	1.29E-96	2.708	0.636	0.017	1.88E-92	6
PI16	3.66E-106	2.632	0.697	0.019	5.33E-102	6
DCN	3.08E-88	2.583	1	0.101	4.48E-84	6
SFRP2	1.51E-105	2.507	0.924	0.052	2.19E-101	6

MGP	7.21E-63	2.430	0.985	0.188	1.05E-58	6
GNLY	9.19E-50	2.701	0.333	0.008	1.34E-45	7
CCL5	1.61E-95	2.617	0.944	0.062	2.35E-91	7
NKG7	8.83E-140	2.590	0.889	0.018	1.28E-135	7
GZMA	2.33E-149	2.395	0.926	0.017	3.38E-145	7
CST7	1.13E-127	2.089	0.944	0.032	1.65E-123	7
GZMK	5.81E-93	2.073	0.722	0.025	8.46E-89	7
IL32	2.05E-72	1.985	0.907	0.082	2.98E-68	7
GZMB	3.31E-99	1.902	0.537	0.004	4.82E-95	7
CD8A	1.37E-104	1.871	0.704	0.017	1.99E-100	7
CD3D	2.85E-83	1.745	0.796	0.046	4.15E-79	7
TIMP1	2.93E-29	3.325	0.963	0.425	4.26E-25	8
TAGLN	1.55E-55	3.002	0.833	0.111	2.25E-51	8
TPM2	1.48E-110	2.969	0.796	0.025	2.15E-106	8
NDUFA4L2	9.12E-92	2.753	0.63	0.016	1.33E-87	8
CCND1	1.09E-59	2.695	0.574	0.032	1.58E-55	8
IGFBP2	1.56E-71	2.674	0.593	0.025	2.26E-67	8
ACTA2	3.56E-56	2.617	0.519	0.027	5.19E-52	8
POSTN	1.34E-54	2.614	0.537	0.031	1.96E-50	8
SPARC	4.58E-53	2.505	0.944	0.167	6.67E-49	8
MYL9	3.80E-97	2.437	0.87	0.044	5.52E-93	8
HLA-DQA1	9.34E-44	2.639	0.63	0.072	1.36E-39	9
HLA-DPA1	1.85E-38	2.366	0.981	0.367	2.69E-34	9
HLA-DPB1	4.68E-33	2.309	0.907	0.31	6.80E-29	9
HLA-DQB1	3.90E-24	1.932	0.63	0.144	5.67E-20	9
HLA-DRA	2.68E-33	1.915	0.981	0.442	3.90E-29	9
CLEC10A	5.18E-44	1.740	0.333	0.011	7.54E-40	9
CD74	2.85E-27	1.737	1	0.605	4.14E-23	9
CST3	3.96E-15	1.698	0.889	0.478	5.76E-11	9
CPVL	4.20E-23	1.653	0.519	0.093	6.10E-19	9
HLA-DRB1	1.68E-10	1.527	0.463	0.155	2.45E-06	9
STC1	1.14E-111	3.281	0.648	0.009	1.66E-107	10
TM4SF1	2.99E-90	2.957	0.981	0.076	4.35E-86	10
ACKR1	1.60E-68	2.696	0.556	0.022	2.33E-64	10
ADAMTS9	2.37E-128	2.537	0.815	0.016	3.45E-124	10
SELE	5.69E-75	2.377	0.5	0.011	8.28E-71	10
AQP1	2.08E-80	2.314	0.648	0.025	3.02E-76	10
GJA1	9.46E-104	2.298	0.741	0.022	1.38E-99	10
IGFBP3	1.88E-31	2.294	0.352	0.025	2.74E-27	10
IL6	2.07E-33	2.259	0.574	0.075	3.01E-29	10
VWF	1.56E-89	2.225	0.722	0.027	2.27E-85	10
TNFRSF13C	3.09E-150	2.177	0.918	0.015	4.50E-146	11
CD79A	8.11E-101	2.094	0.816	0.03	1.18E-96	11

BANK1	1.06E-145	1.780	0.837	0.01	1.55E-141	11
EZR	1.43E-37	1.774	0.959	0.237	2.09E-33	11
MS4A1	7.36E-158	1.748	0.816	0.004	1.07E-153	11
CD37	1.06E-46	1.747	0.98	0.188	1.54E-42	11
NFKBID	9.32E-39	1.714	0.735	0.102	1.36E-34	11
CCR7	2.11E-59	1.654	0.714	0.052	3.08E-55	11
CD83	4.52E-32	1.588	0.878	0.186	6.57E-28	11
ADAM28	1.80E-77	1.571	0.796	0.045	2.61E-73	11
APOD	1.18E-10	3.784	0.347	0.084	1.72E-06	12
CCN1	4.33E-36	2.389	0.653	0.088	6.30E-32	12
LUM	4.25E-37	2.339	0.714	0.103	6.18E-33	12
SFRP4	1.58E-44	2.250	0.673	0.069	2.30E-40	12
DCN	1.18E-50	2.237	0.898	0.123	1.72E-46	12
CCN2	2.35E-29	2.132	0.633	0.104	3.41E-25	12
C11orf96	2.24E-33	2.096	0.673	0.101	3.26E-29	12
INHBA	1.83E-34	2.034	0.469	0.043	2.66E-30	12
SFRP2	1.84E-27	1.991	0.571	0.087	2.68E-23	12
COL1A2	3.44E-35	1.926	0.673	0.095	5.01E-31	12
S100A8	1.17E-41	2.915	0.762	0.092	1.71E-37	13
CXCL8	1.96E-38	2.621	0.976	0.227	2.85E-34	13
EREG	2.04E-53	2.425	0.952	0.111	2.96E-49	13
LUCAT1	2.62E-52	2.413	0.833	0.084	3.81E-48	13
G0S2	2.20E-41	2.412	0.881	0.138	3.20E-37	13
IL1B	1.76E-45	2.316	0.905	0.122	2.57E-41	13
S100A9	9.37E-19	2.298	0.738	0.196	1.36E-14	13
SERPINB2	5.28E-36	2.205	0.238	0.004	7.68E-32	13
AREG	8.92E-25	2.162	0.738	0.162	1.30E-20	13
PTGS2	2.36E-32	2.158	0.548	0.057	3.43E-28	13
GNG11	8.25E-32	2.140	0.524	0.054	1.20E-27	14
RAMP2	4.85E-45	2.112	0.524	0.033	7.06E-41	14
ID1	5.23E-14	2.028	0.286	0.038	7.61E-10	14
IFI27	5.28E-23	2.006	0.595	0.108	7.68E-19	14
HSPG2	1.31E-19	1.904	0.429	0.063	1.91E-15	14
TM4SF1	8.24E-33	1.813	0.714	0.1	1.20E-28	14
CRIP2	1.87E-13	1.754	0.381	0.074	2.72E-09	14
GIMAP7	2.11E-17	1.707	0.381	0.057	3.06E-13	14
VWF	6.56E-26	1.699	0.452	0.048	9.54E-22	14
GIMAP4	2.38E-13	1.646	0.31	0.049	3.46E-09	14

Table S3. Top markers in each cluster among the Mono/Mφ

Gene	p_val	avg_logFC	pct.1	pct.2	p_val_adj	cluster
FN1	3.85E-07	1.186	0.505	0.33	0.00560061	0
MMP9	5.51E-10	1.464	0.308	0.086	8.02E-06	0
COL6A1	2.57E-16	1.832	0.28	0.029	3.73E-12	0
MT1G	1.45E-06	1.194	0.271	0.103	0.0210867	0
H4C3	5.99E-09	1.420	0.196	0.034	8.72E-05	0
COL6A2	5.50E-10	1.469	0.187	0.023	8.00E-06	0
CHI3L1	8.02E-08	1.111	0.15	0.02	0.00116739	0
CKS1B	2.35E-07	1.157	0.14	0.02	0.00341616	0
TOP2A	6.49E-10	1.210	0.131	0.006	9.45E-06	0
PCLAF	5.27E-07	1.085	0.121	0.014	0.00767431	0
SPP1	9.62E-08	0.685	0.785	0.596	0.00139972	0
RPS8	7.17E-07	0.681	0.766	0.713	0.01042588	0
PTMA	2.64E-07	0.480	0.888	0.805	0.00384077	0
TMSB10	1.25E-06	0.374	0.963	0.948	0.01822972	0
TNF.1	1.27E-21	2.460	0.414	0.054	1.85E-17	1
RRAD	1.65E-15	1.731	0.264	0.024	2.40E-11	1
CCL20.1	7.22E-24	1.576	0.632	0.144	1.05E-19	1
PHLDA1.1	2.46E-21	1.458	0.678	0.211	3.58E-17	1
CXCL5	1.36E-09	1.389	0.172	0.019	1.98E-05	1
AC092069.1	1.19E-06	1.354	0.276	0.095	0.01733222	1
CXCL3.1	9.54E-22	1.303	0.77	0.268	1.39E-17	1
TGFBI	1.59E-10	1.287	0.552	0.279	2.31E-06	1
IL1B.1	2.12E-18	1.268	0.69	0.23	3.08E-14	1
CD163.1	4.09E-12	1.163	0.667	0.366	5.95E-08	1
ACKR3.1	1.98E-09	1.112	0.402	0.141	2.88E-05	1
LGMN.1	2.02E-08	1.008	0.575	0.298	0.00029455	1
TFRC.1	5.43E-07	0.983	0.517	0.29	0.00789779	1
CCL4.1	2.46E-11	0.966	0.575	0.233	3.57E-07	1
MGLL	2.81E-06	0.938	0.184	0.043	0.04092451	1
EREG.1	3.49E-11	0.908	0.586	0.238	5.08E-07	1
CTSL.1	3.19E-13	0.807	0.885	0.547	4.65E-09	1
RGCC	2.21E-08	0.806	0.586	0.341	0.00032186	1
FABP5	6.60E-10	0.773	0.793	0.493	9.61E-06	1
G0S2	5.03E-07	0.766	0.506	0.26	0.00732349	1
SELENOP.2	1.21E-27	2.244	0.553	0.078	1.76E-23	2
FOLR2.1	1.40E-10	1.550	0.282	0.059	2.04E-06	2
PDK4	1.34E-06	1.430	0.224	0.062	0.01955275	2
C1QC.1	4.49E-17	1.368	0.647	0.248	6.54E-13	2
C1QB.1	9.27E-16	1.330	0.718	0.332	1.35E-11	2
CTSC.1	5.09E-07	1.138	0.447	0.232	0.0074031	2
PLTP.1	1.86E-07	1.138	0.541	0.321	0.00269964	2

SLC40A1	2.38E-09	1.127	0.153	0.013	3.46E-05	2
C1QA.1	1.50E-08	1.024	0.659	0.394	0.00021807	2
RGS1	4.13E-07	1.012	0.506	0.256	0.00600504	2
LGMN.2	1.93E-06	0.811	0.541	0.307	0.02804195	2
ITM2B.1	2.01E-08	0.811	0.706	0.464	0.0002928	2
HLA-DPB1.2	1.22E-09	0.689	0.718	0.423	1.78E-05	2
CD74.1	2.49E-12	0.660	0.953	0.79	3.62E-08	2
SAT1.1	1.04E-06	0.524	0.882	0.736	0.0150633	2
HLA-DPA1.2	1.10E-08	0.516	0.788	0.531	0.00016068	2
FTL	3.84E-08	0.446	1	0.992	0.00055936	2
B2M.1	1.79E-08	0.420	0.988	0.968	0.00026115	2
FABP4.1	2.46E-26	1.708	0.432	0.032	3.58E-22	3
SCD	2.90E-17	1.394	0.469	0.091	4.22E-13	3
NRP1.2	2.09E-22	1.363	0.556	0.096	3.05E-18	3
SPP1.2	8.74E-25	1.320	0.963	0.571	1.27E-20	3
MMP12.3	1.19E-24	1.295	0.617	0.099	1.73E-20	3
COLEC12.1	3.37E-16	1.200	0.407	0.072	4.91E-12	3
ERRFI1	1.27E-15	1.138	0.358	0.053	1.84E-11	3
SPOCD1	1.58E-11	1.054	0.148	0.005	2.30E-07	3
SDC3	7.15E-14	1.005	0.42	0.091	1.04E-09	3
MT1E.2	3.81E-13	0.975	0.321	0.051	5.54E-09	3
PCOLCE2	3.28E-10	0.959	0.21	0.027	4.78E-06	3
OGFRL1.2	1.46E-10	0.951	0.457	0.147	2.13E-06	3
MMP19.1	1.08E-11	0.940	0.457	0.128	1.58E-07	3
CTSB.2	7.38E-24	0.931	1	0.771	1.07E-19	3
SLC6A8	9.43E-14	0.929	0.198	0.011	1.37E-09	3
LSP1.1	4.88E-10	0.929	0.617	0.28	7.11E-06	3
CD36.3	1.57E-10	0.924	0.642	0.28	2.29E-06	3
IL7R	3.59E-10	0.919	0.247	0.04	5.23E-06	3
ACE	1.33E-11	0.906	0.148	0.005	1.93E-07	3
RND3	7.13E-10	0.903	0.198	0.024	1.04E-05	3
HLA-DQA1.3	5.42E-33	2.470	0.63	0.062	7.88E-29	9
CLEC10A	3.78E-20	1.996	0.333	0.022	5.50E-16	9
HLA-DPA1.3	2.15E-27	1.833	0.981	0.525	3.12E-23	9
FCER1A	2.70E-23	1.817	0.259	0.002	3.93E-19	9
HLA-DPB1.3	8.81E-22	1.791	0.907	0.42	1.28E-17	9
NAPSB	1.54E-16	1.699	0.204	0.005	2.23E-12	9
HLA-DQB1.3	4.56E-16	1.661	0.63	0.172	6.64E-12	9
CST3	3.12E-11	1.626	0.889	0.609	4.54E-07	9
FGL2.2	2.93E-17	1.573	0.5	0.09	4.26E-13	9
HLA-DRB1.1	2.33E-08	1.428	0.463	0.159	0.00033964	9
TCOF1	2.89E-08	1.394	0.204	0.03	0.00042034	9
ATP1B3.1	4.95E-10	1.389	0.667	0.311	7.21E-06	9

SYAP1.1	5.82E-07	1.387	0.426	0.174	0.00846276	9
IFITM3.3	2.49E-09	1.333	0.463	0.144	3.62E-05	9
HLA-DRA.3	1.04E-22	1.323	0.981	0.721	1.51E-18	9
GPAT3	2.73E-07	1.305	0.241	0.052	0.00397018	9
TUBA1A.1	1.15E-09	1.259	0.537	0.199	1.68E-05	9
CD74.2	7.87E-19	1.249	1	0.796	1.15E-14	9
CPVL.2	3.33E-08	1.243	0.519	0.211	0.00048477	9
PPA1	2.05E-09	1.212	0.296	0.057	2.98E-05	9
S100A8.2	2.03E-18	2.497	0.762	0.198	2.95E-14	13
SERPINB2	2.38E-19	2.452	0.238	0.005	3.46E-15	13
PTGS2.1	1.15E-21	2.277	0.548	0.07	1.67E-17	13
VCAN.2	1.90E-21	2.101	0.857	0.249	2.76E-17	13
LUCAT1.1	8.77E-26	2.095	0.833	0.155	1.28E-21	13
G0S2.3	6.72E-22	1.942	0.881	0.249	9.78E-18	13
CXCL8.4	3.38E-21	1.892	0.976	0.461	4.92E-17	13
AREG.2	3.19E-18	1.821	0.738	0.179	4.65E-14	13
TIMP1.1	9.46E-19	1.775	0.976	0.365	1.38E-14	13
EREG.4	7.30E-23	1.763	0.952	0.239	1.06E-18	13
PPIF.1	3.84E-23	1.647	0.905	0.222	5.58E-19	13
FCN1.3	2.30E-29	1.646	0.643	0.058	3.35E-25	13
IL1B.3	1.16E-19	1.634	0.905	0.258	1.69E-15	13
BCL2A1.2	2.95E-16	1.627	0.714	0.191	4.30E-12	13
MCEMP1	2.10E-18	1.563	0.262	0.01	3.06E-14	13
SERPINB9.4	6.48E-12	1.552	0.524	0.121	9.43E-08	13
OLR1.3	3.46E-17	1.451	0.881	0.285	5.03E-13	13
AZIN1-AS1	7.92E-11	1.449	0.262	0.029	1.15E-06	13
ATP2B1-AS1.2	6.50E-23	1.435	0.5	0.046	9.46E-19	13
EHD1.1	1.33E-23	1.392	0.619	0.072	1.94E-19	13

9. POSTER, PRESENTATION AND PUBLICATION

9.1 Posters and Presentation

1. Type: Poster
   Title: Isolation of Primary Adult Smooth Muscle Cells from Patients with Abdominal Aortic Aneurysm disease;
   Event: SFB 1123 Atherosclerosis – Mechanisms and Networks of Novel Therapeutic Targets Annual Retreat 2019;
   Date: Tuesday, 8. October 2019;
   Place: Hotel am Badersee; Am Badersee 1-5, 82491 Grainau.

2. Type: Presentation
   Title: Aortic Intimal Intussusception: A Systematic Review and Pooled Analysis
   Event: Weekly seminar
   Date: Thursday, 12. December 2019;
   Place: Department for Vascular and Endovascular Surgery at the Klinikum rechts der Isar, TUM.

3. Type: Presentation
   Title: Single-Cell RNA Sequencing Revealed Cellular Heterogeneity of Abdominal Aortic Aneurysm in Patient
   Event: 2nd MGC Science Day
   Date: Friday, 16. October 2020;
   Place: Online, Munich

9.2 Lists of Scientific Papers

1. **Zhi-yuan Wu**, Matthias Trenner, Reinier A. Boon, Joshua M. Spin, Lars Maegdefessel*, 2020. Long noncoding RNAs in key cellular processes involved in aortic aneurysms. Atherosclerosis. 292.112-118.

2. Pavlos Tsantilas[1], Shen Lao[1], **Zhiyuan Wu**, Anne Eberhard, Greg Winski, Monika Vaerst, Vivek Nanda, Ying Wang, Yoko Kojima, Jianqin Ye, Alyssa Flores, Kai-Uwe Jarr, Jaroslav Pelisek, Hans-Henning Eckstein, Ljubica Matic, Ulf Hedin, Philip S. Tsao, Valentina Paloschi, Lars Maegdefessel*, Nicholas J. Leeper*, 2020. Chitinase 3 like 1 (CHI3L1) enhances atherosclerotic lesion stability. Cardiovasc Res (*in press*).

3. Daniel Y. Li, Hong Jin, Ekaterina Chernogubova, Greg Winski, Valentina Paloschi, Francesca Fasolo, Sabine Bauer, Susanne Metschl, Hanna Winter, **Zhiyuan Wu**, Marlys L. Koschinsky, Muredach Reilly, Jaroslav Pelisek,

Wolfgang Kempf, Hans-Henning Eckstein, Oliver Soehnlein, Ljubica Matic, Ulf Hedin, Alexandra Bäcklund, Claes Bergmark, Lars Maegdefessel*. Long non-coding RNA MIAT contributes to advanced atherosclerotic lesion formation and plaque destabilization. Manuscript.

4. Albert Busch, **Zhiyuan Wu**, Ekaterina Chernogubova, Daniel Y Li, Hong Jin, Patrick Hofmann, Reinier A Boon, Alexandra Bäcklund, Lars Maegdefessel, Genetic Depletion of Long Non-coding RNA H19 Protects Mice from Elastase-induced Abdominal Aortic Aneurysms. Manuscript.

10. FUNDING

Zhi-Yuan WU is supported by the China Scholarship Council (Award File No. 201806210071). The funders didn't involve in the conception and design, the data collection, analysis and interpretation, the writing or revision of this manuscript and the final decision to publish.

11. ACKNOWLEDGEMENT

Before I came to Germany, I learned a famous German proverb called 'Berg und Tal kommen nicht zusammen, wohl aber die Menschen', which is similar to a Chinese one, 'Fate brings people together no matter how far apart they may be'. I'm so lucky to meet so many excellent people here at Lars group both in Munich and in Stockholm. I'd like to sincerely express my thanks to all the people who are involved in the work of this thesis.

Firstly, I wish to thank my honorific and handsome supervisor, Prof. Dr. Lars Maegdefessel, head of the Vascular Biology and Experimental Vascular Medicine Unit, who is very patient and wealthy in knowledge. He opened a door for me to 'enter the RNA wonderland' in vascular biology. At this team, I'm like standing on the top of the Wallberg am Tegernsee, enjoying the beautiful sceneries of Tegernsee and looking at the distance. His rigorous and prudent attitude towards scientific research showed me the spirit of science, guided me during the past time and I believe I will definitely benefit a lot from this in the future.

I'd also like to thank my mentor, PhD. Alexandra Baecklund, for her suggestions on this thesis-related work. To Prof. Dr. Hans-Henning Eckstein, Head of the Department for Vascular and Endovascular Surgery in Universitätsklinikum rechts der Isar, and his clinical team members like Dr. Matthias Trenner, Dr. Albert Busch, Dr. Christoph Knappich and Dr. Pavlos Tsantilas etc., they have done excellent work on saving life and also providing us with the AAA samples of interest. As a clinical surgeon from China, I also learned a lot from them about the clinical practices here in Germany. And thanks to Dr. Wolfgang Kempf, Head of Munich Vascular Biobank, he managed the connection between the clinical department and the lab quite well and helped a lot on the process of identifying the AAA samples that met the inclusion criteria.

I sincerely appreciate our group leader PhD. Valentina Paloschi, for her help on the scRNA-seq preparations, and her instructing me on the VSMC culture-related techniques, her suggestions on the immunofluorescence staining on the other projects. To my excellent collaborator, Jessica Pauli, PhD. student, she is always enthusiastic and helpful. She did great job on the library preparation of scRNA-seq as well as others. I'd also like to thank Dr. Anne Dueck, postdoc from the Institut für Pharmakologie und Toxikologie at TUM, who helped us with the demultiplexing and with suggestions on the computational analysis.

Except for the help from these people on the scRNA-seq project, I also wish to express my sincere appreciation to my lovely colleagues. Confucius said more than two thousand years ago, 'Even when walking in a party of no more than three, I can always be certain of learning from those I am with' (translated by Arthur Waley). And of course, there are more than three people in our lab for me to learn from, especially when I knew little about translational research work. I'm thankful to PhD. Francesca Fasolo, leader of our RNA team, who reminded me of the details on PCR, gel running and primer design. I want to thank Hanna Winter, PhD. student, who showed me the western blot and paraffin sections. I'd also like to thank Susanne Metschl, PhD student, for sharing me with the immunohistochemistry protocol for the CHI3L1 project and reminding me the details. To Nadiya Glukha, lab technician, thank you for the warm help with the technical details and the daily German talk. Many thanks to PhD. Ekaterina Chernogubova for teaching me with the use of Incucyte machine. To PhD JIN Hong, thank you for encouraging me and the warm help. To Dr. LIU Shengliang and Dr. LAO Shen, thank you for the technical support and suggestions. Thank you all again for the help throughout the project process.

Next, I wish to thank Prof. Dr. LI Yongjun, Head of Department for Vascular Surgery of Beijing Hospital, who encouraged me a lot and shared me with his study experience in Germany and USA, and also discussed with me about the concept of pulmonary thrombosis during the current COVID-19 period. I'd also like to thank my best friends here in Munich, WU Wenkai, DAI Kun, XU Huihui, YUAN Tao, LIU Qiongliang... And thank WANG Zhihua and LU Shu for their nice suggestions for me on the scRNA-seq analysis. It is because of them that the life here is much colorful and meaningful.

Finally, I wouldn't come to Europe without the unconditional support and love of my big family. My grandpa's concern, my parents' weekly WeChat call, care from my elder brother and sister-in-law, joyful 'Uncle' out of my nephew and niece, are all my treasure and keep me walking forward without discouragement. My deepest thank belongs to my girlfriend, YANG Xuetong, who is always on my side even when I'm down. I love you all.

I believe that the experience in both scientific and daily life in Germany will become one of my best precious memories and will definitely guide me well to embrace the coming opportunities and challenges.